CRC REVIVALS

Radiation Dosimetry

Instrumentation and Methods

Second Edition

Gad Shani

CRC Press
Taylor & Francis Group

RADIATION DOSIMETRY

Instrumentation and Methods

Second Edition

Taylor & Francis
Taylor & Francis Group
http://taylorandfrancis.com

RADIATION DOSIMETRY

Instrumentation and Methods

Second Edition

Gad Shani

Department of Nuclear and Biomedical Engineering
Ben Gurion University
Beer Sheva, Israel

CRC Press
Taylor & Francis Group
Boca Raton London New York

CRC Press is an imprint of the
Taylor & Francis Group, an **informa** business

First published 2001 by CRC Press
Taylor & Francis Group
6000 Broken Sound Parkway NW, Suite 300
Boca Raton, FL 33487-2742

Reissued 2018 by CRC Press

© 2001 by Taylor & Francis
CRC Press is an imprint of Taylor & Francis Group, an Informa business

No claim to original U.S. Government works

This book contains information obtained from authentic and highly regarded sources. Reasonable efforts have been made to publish reliable data and information, but the author and publisher cannot assume responsibility for the validity of all materials or the consequences of their use. The authors and publishers have attempted to trace the copyright holders of all material reproduced in this publication and apologize to copyright holders if permission to publish in this form has not been obtained. If any copyright material has not been acknowledged please write and let us know so we may rectify in any future reprint.

Except as permitted under U.S. Copyright Law, no part of this book may be reprinted, reproduced, transmitted, or utilized in any form by any electronic, mechanical, or other means, now known or hereafter invented, including photocopying, microfilming, and recording, or in any information storage or retrieval system, without written permission from the publishers.

For permission to photocopy or use material electronically from this work, please access www. copyright.com (http://www.copyright.com/) or contact the Copyright Clearance Center, Inc. (CCC), 222 Rosewood Drive, Danvers, MA 01923, 978-750-8400. CCC is a not-for-profit organiza-tion that provides licenses and registration for a variety of users. For organizations that have been granted a photocopy license by the CCC, a separate system of payment has been arranged.

Trademark Notice: Product or corporate names may be trademarks or registered trademarks, and are used only for identification and explanation without intent to infringe.

A Library of Congress record exists under LC control number: 00046855

Publisher's Note
The publisher has gone to great lengths to ensure the quality of this reprint but points out that some imperfections in the original copies may be apparent.

Disclaimer
The publisher has made every effort to trace copyright holders and welcomes correspondence from those they have been unable to contact.

ISBN 13: 978-1-138-10559-1 (hbk)
ISBN 13: 978-0-203-71070-8 (ebk)

Visit the Taylor & Francis Web site at http://www.taylorandfrancis.com and the CRC Press Web site at http://www.crcpress.com

Preface

This volume is an updated reference book for medical dosimetry. It evolved from the book *Radiation Dosimetry Instrumentation and Methods* (CRC Press, 1991) published 10 years ago, which contains many of the basic facts of radiation dosimetry techniques. The present book contains developments in the last decade, mainly for medical dosimetry. The two books are complementary.

Radiation dosimetry has made great progress in the last decade, mainly because radiation therapy is more widely used. Every medium to large sized hospital has an oncology department with at least one, generally more, linear accelerators for tumor treatment. Radiation dosimetry has become a common need in the medical world. Medical physicist is now a certified profession and is required by the law in every hospital where radiation treatment is given to patients. One of the main tasks of the medical physicist is to provide the physician with an accurate measurement of the dose delivered to the patient. Several measurement methods were developed together with improved calculation methods, correction factors, and Monte Carlo simulation.

It was the intention of the author to assemble this past decade's developments in one short volume. Unfortunately, because of the vast amount of material, only selected information could be included, and many important developments in this field had to be left out.

The book starts with a short introductory chapter where the basic concepts of radiation and dosimetry are defined. The second chapter deals with basic concepts of radiation dosimetry theory. Electron and photon beams are defined and their interaction with the detector material is described with the consequences of that interaction for dosimetry. Theoretical methods for calculating these effects are discussed.

The main tool in medical dosimetry is the ionization chamber. Because of the importance of an accurate dose measurement, several types of ionization chambers were developed for this purpose in the last decade, having different shapes and dimensions and made of various materials. Application of a dosimeter in a measured system causes perturbation; also the dosimeter itself is not an ideal system. The difference between the measured dose and the calculated one requires the use of correction factors. These are calculated using models developed in the last few years. Ion chambers are also used in portable monitors for area survey; some examples are discussed in Chapter 3.

Chapter 4 deals with the new developments in thermoluminescent dosimetry (TLD). The basic concepts were discussed in *Radiation Dosimetry Instrumentation and Methods* and are not repeated here. New developments of TLD in the last decade are shown with scientific results and applications. Other luminescence dosimetry methods and electron spin resonance dosimetry are included in this chapter.

The new development in film dosimetry is mainly radiochromic film. This new type of film has a high spatial resolution and low spectral sensitivity; therefore, it is useful for dose distribution measurement. Again, the basic aspects of film dosimetry are not repeated in Chapter 5.

Some progress in calorimetry dosimetry was made. However, the two materials used for dose measurement are still water and graphite, because of the similarity between these materials' interaction with radiation to that of tissue. Calorimetry dosimetry and chemical dosimetry are discussed in Chapters 6 and 7, respectively.

Solid-state dosimetry has made considerable progress in the last decade. First, the use of diamonds became popular, mainly because diamonds are made of pure carbon and are close to tissue equivalent. Also as a perfect crystal, a diamond makes a good solid-state detector. The development of solid-state devices for electronics found its way to radiation dosimetry too. MOSFET and other devices are small and capable of detecting very low currents when used as solid-state detectors. Another way of using them: radiation effect on the device's performance is an indication of the dose absorbed.

Chapter 9 deals with a new development in radiation dosimetry, a three dimensional dosimeter. Detection of changes taking place in gel is a measure of the dose absorbed. One way to detect changes is by introducing ferrous sulfate to the gel and measuring light absorption following the irradiation, as done with the Fricke dosimeter. Another way is by changing the gel properties with radiation, then using three dimensional nuclear magnetic resonance (NMR) to measure the changes. It seems to give a good solution to the problem of three dimensional dosimetry, done in one measurement. This new dosimetry method is at its early stages of application.

Chapter 10 deals with neutron dosimetry. As is well known, neutron detection cannot be done by direct ionization; as in other kinds of radiation, secondary radiation is used. Neutron measurement is done using all the techniques used for other radiation measurements, i.e., ionization chamber, scintillator (TLD for dosimetry) and solid-state detectors. In addition, methods specific to neutron measurement include activation analysis and track detector. Because neutron

interactions with matter are different from interactions with other forms of radiation, it is important for neutron dosimetry to use detectors made of tissue equivalent materials. When gamma radiation is present, pair detectors are used, and the gamma dose is subtracted. When TLD is used, it should contain isotopes with high cross-section for neutron interaction, such as Li^6 for thermal neutrons.

A few new developments in neutron dosimetry came about in the last decade. One of them is the superheated drop detector in which the number of bubbles formed in the liquid is a function of neutron dose. Solid state diodes were developed with polyethylene or boron converters. Gamma dose is subtracted in these detectors by the pulse shape discrimination technique.

Bonner sphere was developed many years ago as an area monitor. In the last decade, better designs were made with better energy response.

The book was written for medical physicists, engineers, and advanced dosimetrists. As mentioned above, it contains only the last decade's developments. If more basic data or methods are sought, the reader should refer to the book *Radiation Dosimetry Instrumentation and Methods.*

The Author

Gad Shani, Ph.D., is a professor in the department of nuclear engineering and the head of the biomedical engineering program at Ben Gurion University, Beer Sheva, Israel. Professor Shani received his B.Sc. degree in electrical engineering and M.Sc. degree in nuclear science at the Technion Israel Institute of Technology in 1964 and 1966, respectively, and his Ph.D. in nuclear engineering from Cornell University, Ithaca, New York. On the faculty at Ben Gurion University since 1970, Dr. Shani was one of the founders of the department of nuclear engineering and the head of the department from 1980 to 1984. Since 1994, he has served as the head of the biomedical engineering program.

Professor Shani is the incumbent of the Davide and Irene Sala Chair in Nuclear Engineering and the head of the Center for Application of Radiation in Medicine. He is a member of the International Euroasian Academy of Science. Professor Shani was a visiting scientist in many laboratories around the world, including the KFA in Germany as a winner of the European Community grant; in Harwell, England as a winner of the British Royal Society grant; at McMaster University in Canada; and at UCLA in the U.S. He spent sabbatical years at the University of California, Santa Barbara, Ohio State University, and Brookhaven National Laboratory (BNL) where he was a collaborator for the last 10 years. Additionally, he spent a few months every year at BNL doing research in the fields of neutron capture therapy, synchrotron radiation, and other methods for cancer treatment with radiation.

Professor Shani's field of scientific activity over the years spans a wide area, including neutron physics, reactor physics, nuclear instrumentation, dosimetry, and medical physics. His professional affiliations include the American Nuclear Society, Israel Nuclear Society (council member), Israel Ecology Society, Israel Society for Medical and Biomedical Engineering (council member), International Federation for Medical and Biomedical Engineering, Israel Society of Medical Physics, Israel Society of Radiation Research, and International Society for Neutron Capture Therapy. He has published about 150 papers in journals and meeting proceedings, authored 4 books, and co-authored 2 books.

Taylor & Francis
Taylor & Francis Group
http://taylorandfrancis.com

Contents

Chapter 1
Introduction 1

Chapter 2
Theoretical Aspects of Radiation Dosimetry 13

Chapter 3
Ionization Chamber Dosimetry 85

Chapter 4
Thermoluminescent Dosimetry 221

Chapter 5
Film Dosimetry 301

Chapter 6
Calorimetry 331

Chapter 7
Chemical Dosimetry 349

Chapter 8
Solid-State Dosimeters 361

Chapter 9
Gel Dosimetry 401

Chapter 10
Neutron Dosimetry 423

Index 477

Taylor & Francis
Taylor & Francis Group
http://taylorandfrancis.com

1 Introduction

CONTENTS

I. Units and Definitions 1
II. Absorbed Dose in Terms of Exposure and Stopping Power 3
III. Linear Energy Transfer 4
A. Dose-Equivalent Quantities 4
B. Dose Equivalent 5
C. Ambient Dose Equivalent 5
D. Directional Dose Equivalent 5
IV. Dosimetry Methods 5
A. Ionization Method 5
B. Chemical Methods 5
C. Calorimetric Methods 5
D. Thermoluminescence Methods 6
V. Gamma Dosimetry 6
A. Point Source Dose 6
B. First Collision Dose 6
VI. Beta Dosimetry 7
VII. Neutron and Heavy Particles Dosimetry 7
A. Neutron Dosimetry 7
B. Heavy Particles 8
VIII. Biological Dosimetry 8
IX. Cavity Theory 10
References 10

I. UNITS AND DEFINITIONS

The energy imparted by ionizing radiation to matter of a given mass is the fundamental quantity of radiation dosimetry. Radiation field can be described by the average number of rays (or particles) per unit area, per unit time at each point. The rays can be in a parallel beam at angle θ to the plane or moving at all directions. In the second case the examined surface should be a sphere. If the examined area is a circle with area Δa (or one quarter of the sphere area) and the number of rays crossing it at time Δt is ΔN, then the flux density is given by

$$\Phi = \frac{\Delta N}{\Delta a \Delta t} \tag{1.1}$$

and integration over time gives the fluence

$$\Phi = \frac{\Delta N}{\Delta a} \tag{1.2}$$

Another way to deal with a radiation field is by summing the kinetic energy of all the particles entering the sphere:

$$\Delta E = \sum_i T_i \tag{1.3}$$

where T_i is the kinetic energy of the ith ray or particle. The intensity is given by

$$I = \frac{\Delta E}{\Delta a \Delta t} \tag{1.4}$$

If there is more than one kind of ray or particle, the flux density and the energy fluence can be calculated for each separately. If the particles (or rays) have different energies within a range, the flux density will be the integration of the distribution (or spectrum) over the energy range. When a beam of radiation encounters matter, it will be attenuated by the interaction with the matter. The attenuation can be measured by the reduction in number of rays or panicles, or by the reduction of the total beam energy.

The official units used in health physics and dosimetry are those agreed upon by the International Commission

on Radiological Units and Measurements (ICRU). [1] In radiation protection the term for the linear energy transfer dependent factor is the quality factor (QF) by which absorbed doses are multiplied to obtain a quantity expression of the irradiation incurred on a common scale. The distribution factor (DF) expresses the nonuniformity effect of the irradiation. The product of the absorbed dose (D) and the two factors above is the dose equivalent

$$\mathrm{DE} = \mathrm{D} \times \mathrm{QF} \times \mathrm{DF} \quad (\mathrm{Sv}) \tag{1.5}$$

The units generally used in dosimetry are gray (Gy) for absorbed dose, roentgen (R) for exposure, and curie (Ci) for activity. Definitions of some terms used in dosimetry are listed below:

- Direct ionizing particles—charged particles having sufficient kinetic energy to produce ionization
- Indirect ionizing particles—uncharged particles that can produce ionizing particles
- Ionizing radiation—radiation consisting of directly and indirectly ionizing particles
- Energy imparted by ionizing radiation—the difference between the sum of energies of ionizing particles entering a certain volume and the sum of energies leaving the volume, less the energy spent in increasing any rest mass
- Absorbed dose—the quotient of the energy imparted by ionizing radiation and the mass of this volume:

$$D = \frac{\Delta E}{\Delta m} \tag{1.6}$$

  The units of absorbed dose are 1 Gy = 100 rad where 1 rad = 100 erg/gm.
- Absorbed dose rate—the quotient of the incremental absorbed dose and the absorption time:

$$\dot{D} = \frac{\Delta D}{\Delta t} \tag{1.7}$$

  The units can be Gy/min, Gy/sec, etc.
- Particle fluence—the quotient of the number of panicles ΔN that enter a sphere of area $4\Delta a$ (a test sphere) and the area Δa (the sphere cross-section area):

$$\Phi = \frac{\Delta N}{\Delta a} \tag{1.8}$$

- Particle flux rate—the incremental particle flux per time interval; ϕ denotes flux distribution with respect to energy, direction, etc.:

$$\Phi = \frac{\Delta \phi}{\Delta t} \tag{1.9}$$

- Energy fluence—the incremental kinetic energy of all particles entering the sphere of area $4\Delta a$ (cross-section Δa) per cross-section area:

$$F = \frac{\Delta E}{\Delta a} \tag{1.10}$$

- Energy flux density—the incremental energy fluence per time interval:

$$I = \frac{\Delta F}{\Delta t} \tag{1.11}$$

- Kerma—the incremental kinetic energy of all charged particles liberated by ionizing particles in a volume element divided by the mass of this volume element:

$$K = \frac{\Delta E}{\Delta m} \tag{1.12}$$

- Kerma rate—incremental kerma in time interval Δt:

$$\frac{\Delta K}{\Delta t} \tag{1.13}$$

- Exposure—the ratio between the sum of secondary electrical charge (ions of one sign produced when electrons produced by photons are stopped) in a volume element of air to the mass of that volume:

$$X = \frac{\Delta Q}{\Delta m} \tag{1.14}$$

  The unit of exposure is roentgen: 1 R = 2.58×10^{-4} Cb/kg. (This is identical to 1 ESU per 1 cc [0.001293 g] of air.)
- Exposure rate—the incremental exposure in time interval Δt:

$$\frac{\Delta X}{\Delta t} \tag{1.15}$$

  The units are R/sec (or R/min, etc.)
- Mass attenuation coefficient—the property of the material defined by

$$\frac{\mu}{\rho} = \frac{1}{\rho N} \frac{dN}{dl} \tag{1.16}$$

for indirectly ionizing particles; ρ is the material density, N is the number of particles incident normal to the material, and dN is the number of particles interacting in thickness dl.

- Mass energy transfer coefficient—the property of the material defined by

$$\frac{\mu_k}{\rho} = \frac{1}{\rho E}\frac{dE}{dl} \tag{1.17}$$

where E is the sum of kinetic energies T_i of indirectly ionizing particles meeting normally on the material of density ρ. dE is the sum of the kinetic energies of all the charged particles liberated in thickness dl. One use of this quantity is the ratio between fluence and kerma:

$$F = K\frac{\mu_k}{\rho} \tag{1.18}$$

- Mass absorption coefficient—the property of the material defined as

$$\mu_{en} = \frac{\mu_k}{(1-g)} \tag{1.19}$$

where g is the part of the energy of the secondary charged particles lost by *bremsstrahlung*.

- Mass stopping power—the property of the material defined as

$$S = \frac{dE_s}{dl} \tag{1.20}$$

where dE_s is the average energy lost by a charged particle traversing the length dl.

- Linear energy transfer—the energy imparted from charged particles to the medium

$$L = \frac{dE_L}{dl} \tag{1.21}$$

where dE_L is the average local energy imparted when the particle travels a distance dl.

- Average energy expended in a gas per ion pair formed—

$$W = \frac{E}{N_w} \tag{1.22}$$

where E is the particle initial energy and N_w is the average number of ion pairs formed by complete stopping of the particle. Activity units are

$$1\ \text{Ci} = 3.7 \times 10^{10}\ \text{sec}^{-1}$$

II. ABSORBED DOSE IN TERMS OF EXPOSURE AND STOPPING POWER

When the exposure is 1 R, the energy absorbed in air is 87.7 erg/g. The absorbed dose is

$$D_{air} = 0.877\ R\ \text{rad} \tag{1.23}$$

where R is the number of roentgens. If the medium is not air, then

$$D_m = 0.877\ R\ \frac{\mu_{en}/\rho_m}{\mu_{en}/\rho_{air}} = fR\ \text{rad} \tag{1.24}$$

where f is the number of rad per roentgen in the medium.

When the spectrum is continuous, integration should be carried out:

$$D = \int_0^\infty R(E)f(E)\,dE \tag{1.25}$$

and

$$R = \int_0^{E_{max}} R(E)\,dE \tag{1.26}$$

The absorbed dose for a charged particle can be expressed in terms of the stopping power. If the stopping power is

$$S(T) = \frac{dT}{dx} \tag{1.27}$$

and the particle fluence is $\phi(E)$, then using the definition,

$$D = \frac{\Delta E}{\Delta m} \tag{1.28}$$

$$D = \frac{1}{\rho}\int_0^{T_{max}} S(T)\phi(T)\,dt \tag{1.29}$$

where ρ is the stopping material density and the charged particles impinge perpendicular to the area.

The mean absorbed dose, D_T, in a specified tissue or organ, T, is given by

$$D_T = \frac{1}{m_T}\int_{m_T} D\,dm \tag{1.30}$$

where m_T is the mass of the tissue or organ and D is the absorbed dose in the mass element dm. The mean absorbed dose, D_T, in a specified tissue or organ equals the ratio of

the energy imparted, ε_T, to the tissue or organ, and m_T, the mass of the tissue or organ.

III. LINEAR ENERGY TRANSFER

Linear energy transfer (LET) denotes the energy lost by a charged particle per unit distance of medium traversed:

$$L = \frac{dE_L}{dl} \tag{1.31}$$

where dE_L is the average energy locally imparted to the medium. When a nonmonoenergetic radiation interacts with material, there is a distribution of LET. If the distribution of tracks is $T(L)$, then the average LET can be defined as:

$$\overline{L_T} = \int_0^{L_{max}} T(L) L \, dL \tag{1.32}$$

or dose average

$$\overline{L_D} = \int_{L_{min}}^{L_{max}} D(L) L \, dL \tag{1.33}$$

Charged particles lose energy by colliding with the atomic electrons and transferring energy to them. This energy can be half the partial energy if the particle is an electron and four times the relative mass between the electron and the particle for heavy particles. The scattered electrons that are δ-rays form their own track, which might branch to a ternary track. δ-rays of energy above 100 eV are generally considered separate particles (in some cases higher energy is taken). The selection of the lower limit of δ-rays affects the LET of the original particle and makes the calculation complicated.

Energy transfer of heavy charged particles (HCP) to nm-size targets have been investigated by Iwanami and Oda [2], taking into account δ-ray generation by HCP as well as associated δ-rays. The energy transfer into the target is mainly due to ionizing collisions of HCP with matter. Secondary electrons generated by ionizing collisions within the target, whose ranges are much larger than the target size, deposit almost all of their energy outside the target. The ionizing collisions generating such secondary electrons are therefore excluded from the energy transferred into the target and are regarded as generating a new electron fluence. The energy of these electrons is greater than the cutoff energy for δ-rays, Δ. Secondary electrons with energy less than Δ dissipate their energy locally at their production site. ICRU [3] defined two kinds of LET: unrestricted and restricted. The unrestricted LET, L_∞, is the quotient of dE and dl, where dE is the mean energy lost by a charged particle due to collisions with electrons in traversing a distance dl; thus,

$$L_\infty = \frac{dE}{dl} \tag{1.34}$$

L_∞ does not take into account δ-ray production. The restricted LET, L_Δ, is the quotient of dE by dl, where dE is the energy lost by a charged particle in traversing a distance dl due to those collisions with electrons in which the energy loss is less than the restricted energy Δ:

$$L_\Delta = \left(\frac{dE}{dl}\right)_\Delta \tag{1.35}$$

Where Δ is the cut-off energy for δ-rays and restricted energy of L_Δ,

A simplified parameter, the event size Y, was suggested by Rossi. [4] It is the ratio between the energy deposited in a small sphere by the primary and secondary particles to the sphere diameter d:

$$Y = \frac{E}{d} \tag{1.36}$$

The complication here is that Y requires additional parameter d.

A distribution of event size Y can be found as a distribution of the LET or track length. The relation between the distribution of the absorbed dose in Y, $D(Y)$, and the distribution in L, $D(L)$, can be found by examining the relation of a track length within a sphere and the sphere diameter d:

$$D(Y) = \frac{3Y^2}{L^2} \tag{1.37}$$

where Y is idealized by assuming that the tracks are straight lines, the energy loss is uniform, and Y is independent of d. $Y \leq L$ since Y_{max} occurs along the diameter, at which position $Y = L$. It is also possible to write

$$D(Y) = 3Y^2 \int_Y^{L_{max}} \frac{D(L)}{L^3} \, dL \tag{1.38}$$

A. Dose-Equivalent Quantities

A quality factor, Q, is introduced to weight the absorbed dose for the biological effectiveness of the charged particles producing the absorbed dose. It is formulated to take account of the relative effectiveness of the different types of ionizing radiation at the low exposure levels encountered in routine radiation protection practice. The quality

factor, Q, at a point in tissue is given by

$$Q = \frac{1}{D}\int_L Q(L)D_L\,dL \tag{1.39}$$

where D is the absorbed dose at that point, D_L is the distribution of D in linear energy transfer L, and $Q(L)$ is the corresponding quality factor at the point of interest. The integration is to be performed over the distribution D_L, due to all charged particles, excluding their secondary electrons.

B. Dose Equivalent

The dose equivalent, H, is the product of Q and D at a point in tissue, where D is the absorbed dose and Q is the quality factor at that point; thus,

$$H = QD \qquad \text{(Sv)} \tag{1.40}$$

The quantity dose equivalent is defined for routine radiation-protection applications. The dose equivalent, H, at a point is given by

$$H = \int_L Q(L)D_L\,dL \tag{1.41}$$

where $Q(L)$ is the quality factor for particles with linear energy transfer L and D_L is the spectral distribution, in terms of L, of the absorbed dose at the point.

C. Ambient Dose Equivalent

The ambient dose equivalent, $H^*(d)$, at a point in a radiation field is the dose equivalent that would be produced by the corresponding expanded and aligned field in the ICRU sphere [5] at a depth d on the radius opposing the direction of the aligned field. [6]

For strongly penetrating radiation, a depth of 10 mm is currently recommended. The ambient dose equivalent for this depth is then denoted by $H^*(10)$. For weakly penetrating radiation, depths of 0.07 mm for the skin and 3 mm for the eye are employed, with analogous notation.

Measurement of $H^*(10)$ generally requires that the radiation field be uniform over the dimensions of the instrument and that the instrument have an isotropic response.

D. Directional Dose Equivalent

The directional dose equivalent, $H'(d, \Omega)$ (Sv), at a point in a radiation field is the dose equivalent that would be produced by the corresponding expanded field in the ICRU sphere at a depth d on a radius in a specified direction, Ω. The ICRU sphere is a 30-cm-diameter tissue-equivalent sphere with a density of 1 g cm^{-3} and a mass composition of 76.2% oxygen, 11.1% carbon, 10.1% hydrogen and 2.6% nitrogen.

IV. DOSIMETRY METHODS

A. Ionization Method

The most widely used method of dosimetry is based on ionization. The number of ion pairs produced is

$$I = \sum_i \int_B^\infty \frac{\varepsilon_i n_i(E)\,d\varepsilon_i}{w(\varepsilon_i)} \tag{1.42}$$

where B is the lower limit of energy loss and $w_i(\varepsilon_i)$ is the energy required for a particle of type i at energy ε to produce an ion pair. Since for many gases w is independent of i and ε, $I = \varepsilon T/w$.

When measurement of the dose at a specific position is required, the detector dimensions must be small compared to the attenuation length of the primary radiation. If this is impossible, the first collision dose in the detector must be the same as in the medium, or, at least, the ratio between the first collision doses in the two materials must be independent of energy. It is always required that the ratio of the stopping powers in the two materials is independent of energy.

B. Chemical Methods

In some systems the chemical composition is changed by the absorbed radiation (including photographic film). If Y is the observed chemical change, then

$$Y = \sum_i \int_0^\infty \varepsilon_i n_i(\varepsilon_i, E)G_i(\varepsilon_i)\,d\varepsilon_i \tag{1.43}$$

where $G_i(\varepsilon_i)$ is the yield per unit energy absorbed. If G is independent of particle type and ε_i, then

$$Y = G\varepsilon T \tag{1.44}$$

C. Calorimetric Methods

The radiation energy absorbed in the dosimeter changes into thermal energy and raises the dosimetry temperature. The temperature change is given by

$$\Delta T = \frac{1}{c}\sum_i \int_0^\infty \varepsilon_i n_i(\varepsilon_i, E)F_i(\varepsilon_i)\,d\varepsilon_i \tag{1.45}$$

where $\varepsilon_i n_i(\varepsilon_i, E)\,d\varepsilon_i$ is the amount of energy absorbed in a unit mass. $F_i(\varepsilon_i)$ is the fraction of charged particle energy

that is degraded to heat. c is the thermal capacity of the substance. $F_i(\varepsilon_i)$ is approximately constant near unity so that

$$\Delta T = \frac{\varepsilon T}{c} \tag{1.46}$$

D. Thermoluminescence Methods

When radiation is absorbed by an impure crystal, some of the electrons are trapped in the levels created within the forbidden gap. When those electrons are forced by heat to return to the valence band, their energy is emitted as light. The total amount of light emitted is proportional to the dose absorbed in the crystal:

$$L = \sum_i \int_B^\infty \varepsilon_i n_i(E)\, d\varepsilon_i \tag{1.47}$$

where L is the total amount of light, ε_i is the light photon energy, and n_i is the number of light photons. B is the lower limit of light detection.

V. Gamma Dosimetry

A. Point Source Dose

If we define dose rate as the energy absorbed per unit volume per unit time, it is given that

$$D' = \mu I(E, r) \tag{1.48}$$

where $I(E, r)$ is the flux density of energy E at a distance r from a point source. If the point source strength is S, then

$$I(E, r) = \frac{S}{4\pi r^2} \tag{1.49}$$

when no attenuation in the surrounding material is assumed. With attenuation the flux is

$$I(E, r) = \frac{S}{4\pi r^2} e^{-\mu r} \tag{1.50}$$

For the dose rate to be in units of energy absorbed per unit time as defined above, the source must be expressed in units of energy

$$S = cE \text{ MeV/s} \tag{1.51}$$

where c is the source intensity in disintegration per second and E is in MeV. If the source strength c is expressed in curie, then

$$S = 3.7 \times 10^{10}\, cE \tag{1.52}$$

and the dose rate is

$$D' = 2.96 \times 10^9 \mu cE \frac{e^{-\mu r}}{r^2} \frac{\text{MeV}}{\text{cm}^2/\text{s}} \tag{1.53}$$

The total dose is obtained by time integration of the dose rate:

$$D = \int D'\, dt \tag{1.54}$$

or, if the dose rate is constant,

$$D = D't \tag{1.55}$$

Radioactive isotopes are an exponentially decaying source, so integration must be carried out for at least short-lived isotopes. When the source is other than a point source, the flux must be calculated accordingly. Self absorption should sometimes be included.

For high-dose measurement the following dosimeters are used: calorimeters, alanine/electron spin resonance (ESR) systems, liquid solutions (Fricke, ceric-cerous, dichromate), and polymer systems (polymethyl methacrylate, cellulose triacetate, radiochromic films and optical waveguides).

B. First Collision Dose

When a beam of ionizing radiation meets with a small mass so that the attenuation is small, the dose is referred to as first collision dose. It is expressed in terms of the energy imparted to a unit mass of the material per unit time per unit flux at the incident beam. An expression for the first collision dose for gamma rays of energy E is given by

$$D(E) = 1.602 \times 10^{-8} \sum_i N_i \{\tau_i(E)\varepsilon_{pe}(E) + \sigma_i(E)\varepsilon_c + \kappa_i(E)\varepsilon_{pp}\} \tag{1.56}$$

where $D(E)$ is in rad/(photon/cm^2); N_i is the number of atoms of the ith element per gram of material; $\tau_i(E)$, $\sigma_i(E)$, and $\kappa_i(E)$ are the photoelectric, compton, and pair production cross sections, respectively, in cm^2/atom of the ith element; and ε is the average kinetic energy transferred to the electron (or positron) in the effects taking place (*pe* is photoelectric, *c* is compton, and *pp* is pair production). In the photoelectric effect, $\varepsilon_{pe} = E - E_B$, where E_B is the electron binding energy. The kinetic energy transferred to the electron in the compton effect is

$$E_c = \frac{aE(1 - \cos\phi)}{1 + \alpha(1 - \cos\phi)} \tag{1.57}$$

where $\alpha = E/0.511$ MeV and ϕ is the Compton scattered photon angle.

For the pair production $\varepsilon_{pp} = E - 1.022$. The summation in Equation (1.56) is over all elements in the absorbing material. The factor 1.602×10^{-8} converts MeV/gr to rad. At low energy the main effect is the photoelectric effect. The cross section is decreased when the energy is increased, and it has the Z^5 dependence. At energies above 0.2 MeV, the main interaction is the Compton effect and then the pair production. Both cross sections are relative to the number of electrons per unit volume; hence, the difference between the different materials is small.

VI. BETA DOSIMETRY

There are several methods of calculation of beta dose and different applications of these methods according to the different source geometry. A point source dose rate can be calculated with the Loevinger formula [7]:

$$D'(r) = \frac{KC}{(\mu r)^2}\left\{c\left[1 - \left(\frac{\mu r}{c}\right)e^{(1-\mu r/c)}\right] + \mu r e^{(1-\mu r)}\right\} \tag{1.58}$$

where $D'(r)$ is the beta dose rate in rad per hour at distance r from the point source, r is measured in gr/cm^2, C is the source intensity in curies, c is a parameter dependent on the beta maximum energy (dimensionless), μ is the absorption coefficient in cm^2/gr, and K is a normalization constant

$$K = \frac{1.7 \times 10^5 \rho^2 \mu^3 E_{av}}{[3c^2 - e(c^2 - 1)]} \frac{\text{rad/h}}{\text{curie}} \tag{1.59}$$

where ρ is the absorber density, e is the mathematical e, and E_{av} is the beta average energy. The value of c in air is $3.11e^{-0.55E_{max}}$ and in tissue, $c = 2$ for $0.17 \leq E_{max} < 0.5$ MeV, $c = 1.5$ for $0.5 \leq E_{max} < 1.5$ MeV, and $c = 1$ for $1.5 \leq E_{max} < 3.0$ MeV. μ in air is given by

$$\mu = \frac{16(2 - E_{av}/E^*_{av})}{(E_{max} - 0.036)^{1.4}} \text{ cm}^2/\text{gr} \tag{1.60}$$

E^*_{av} is called the hypothetical average beta energy per disintegration for a hypothetical forbidden beta disintegration having the same E_{max} as an allowed beta decay transition in the same Z element. For allowed spectra, $E_{av}/E^*_{av} = 1$.

Other simple expressions for beta dose rate calculation are available. In analogy to gamma point source dosimetry, the following equation can be used:

$$D'(r) = 2.14 \times 10^6 \rho^2 \frac{\mu}{\rho} C E_{av} \frac{e^{-\mu r/\rho}}{4\pi r^2} \frac{\text{rad}}{\text{h}} \tag{1.61}$$

for C in curies, E_{av} in MeV, ρ in gr/cm^3, $\mu/\rho = 17E_{max}^{-1.14}$ cm^2/gr, and r in gr/cm^2. Expressions for other source geometries can be found in Fitzgerald et al. [8]

VII. NEUTRON AND HEAVY PARTICLES DOSIMETRY

A. Neutron Dosimetry

Neutron dosimetry is done by transforming the number density of neutrons (or neutron flux) to dose. This is done by using the equation

$$D'(r,E) = K\phi(r,E)\left[\Sigma_s(E)\frac{AE}{(A+1)^2} + \Sigma_{n,\gamma}(E)E_\gamma B\right] \tag{1.62}$$

where $D'(r, E)$ is the dose rate in rad/h, K is a conversion factor

$$K = 5.76 \times 10^{-5} \frac{\text{rad}}{\text{h}} \Big/ \frac{\text{Mev}}{\text{cm}^3\text{s}}$$

ϕ (r, E) is the neutron flux in n/cm^2 sec, A is the atomic mass of the target nucleus, E_γ is the radioactive capture gamma-photon energy in MeV, and B is a factor representing the fraction of radioactive capture gamma-photon energy absorbed in the neighborhood of the capture. $A/(A + 1)^2$ is the fraction of incident neutron energy imparted to the recoil nucleus of mass A. Σ_s is the scattering cross section and $\Sigma_{n,\gamma}$ is the (n, γ) reaction cross section. If any other reaction in addition to scattering and radiation capture takes place, the energy transferred to the substance should be included.

The energy transferred to the substance after neutron collision (first collision dose) is given by

$$D(E) = 1.602 \times 10^{-8} \sum_i \sum_j N_i \sigma_{ij}(E) \varepsilon_{ij}(E) \tag{1.63}$$

where N_i is the number of nuclei of type i per gram of substance, σ_{ij} is the cross section of the ith kind of nucleus for the reaction in which particles of type j are produced, and ε_{ij} is the average kinetic energy of the jth particle emitted by the ith nucleus.

In elastic scattering the secondary panicle is the scattered neutron, and for the isotropic case,

$$\varepsilon_{ij} = \frac{2mM_iE}{(m + M_i)^2} \tag{1.64}$$

where m is the neutron mass, M_i is the nucleus mass, and E is the neutron energy.

For an unisitropic scattering, the last expression should be multiplied by $1 - f_{li}(E)$, where $f_{li}(E)$ is given by the expansion of the elastic cross section

$$\sigma_{el}(E, \Theta) = \frac{\sigma_{el,0}(E)}{4\pi}\sum_{l=0}^{\infty}(2l + 1)f_{l,i}(E)P(\cos\Theta) \tag{1.65}$$

P is the Legendre polynomial.

In the case of nuclear reaction,

$$\varepsilon_{ij}(E) = E + Q_{ij} \quad (Q_{ij} + E > 0) \tag{1.66}$$

where Q_{ij} is the reaction Q value.

B. Heavy Particles

The introduction of heavy particles (hadrons) into radiation therapy aims at improving the physical selectivity of the irradiation (e.g., proton beams) or the radiobiological differential effect (e.g., fast neutrons) or both (e.g., heavy ion beams). Each of these therapy modalities requires several types of information; absorbed dose measured in a homogeneous phantom in reference conditions; dose distribution computed at the level of the target volume(s) and the normal tissues at risk; radiation quality from which an evaluation on the RBE could be predicted; and RBE measured on biological systems or derived from clinical observation. The single beam isodoses and thus the dose distributions are similar in neutron and photon therapy. Similar algorithms can then be used for treatment planning and the same rules can be followed for dose specification for prescribing and reporting a treatment. In hadron therapy, the RBE of the different beams raises specific problems. For fast neutrons, the RBE varies within wide limits (about 2 to 5) depending on the neutron energy spectrum, dose, and biological system. For protons, the RBE values range between smaller limits (about 1.0 to 1.2). A clinical benefit is thus not expected from RBE differences. However, the proton RBE problem cannot be ignored since dose differences of about 5% can be detected clinically in some cases. The situation is most complex with heavy ions since the RBE variations, as a function of particle type and energy, dose, and biological system, are at least as large as for fast neutrons. In addition, the RBE varies with depth. Radiation quality thus has to be taken into account when prescribing and reporting a treatment. This can be done in different ways: description of the method of beam production; computed LET spectra and/or measured microdosimetric spectra at the points clinically relevant; or RBE determination. The most relevant data are those obtained for late tolerance of normal tissues at 2 Gy per fraction ('reference RBE'). Combination of microdosimetric data and experimental RBE values improves the confidence in both sets of data.

VIII. BIOLOGICAL DOSIMETRY

When dose to radiation workers or to patients is a concern, biological dosimetry is the most accurate dosimetry technique. In this way the radiation effect on the human body is measured directly without the intermediary of a technical device. No interpretation of physical or chemical phenomena taking place in the dosimeter is needed, nor is there a need for corrections.

Chromosome aberration analysis is recognized as a valuable dose-assessment method which fills a gap in dosimetric technology. Detection of chromosomal aberrations

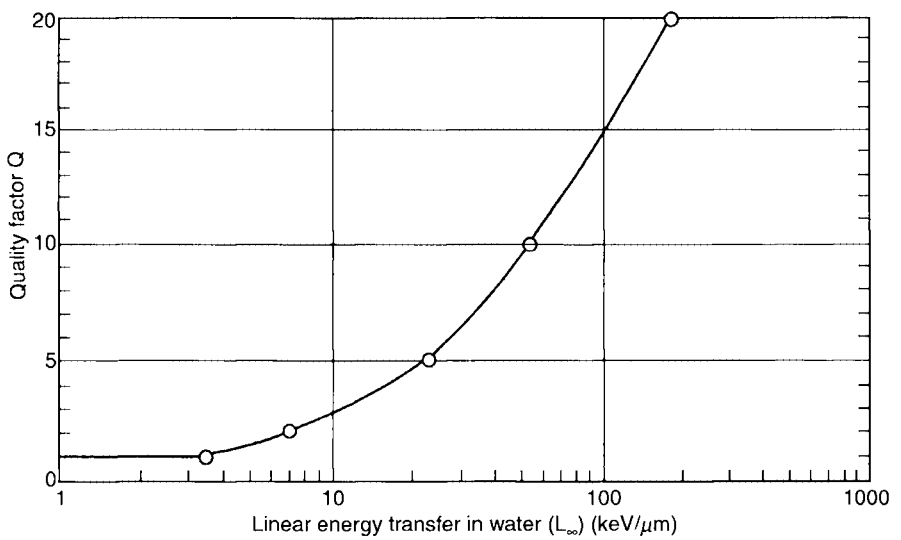

FIGURE 1.1 Quality factor as a function of linear energy transfer in water (L_∞).

in the peripheral blood lymphocytes of exposed persons is the most fully developed biological indicator of exposure to ionizing radiation. By using a distribution analysis of the aberrations, it is possible to estimate the proportion of the body exposed and the average dose absorbed by the irradiated fraction.

The influence of the microscopic distribution of the absorbed energy on the detriment is taken into account by the use of the quality factor, Q.

The ICRP [9] recommends the following approximations for the average value of Q:

- X-rays, γ-rays and electrons: 1
- Thermal neutrons: 4.6
- Other neutrons: 20
- Protons and single-charged particles of unknown energy and rest mass $\geq$ 1 : 10
- α-particles and multiple-charged particles of unknown energy: 20

The dependence of Q on LET is shown in Figure 1.1.

The RBE varies with the LET such that a hump-shaped response curve is obtained. A generalized curve is shown in Figure 1.2.

In order to produce a dicentric aberration, DNA damage must be induced in the two unreplicated chromosomes involved such that the damaged chromosomes can undergo exchange.

As the dose increases, the contribution of two track-induced dicentrics will also increase. Thus, the dose-response curve for X-ray-induced dicentrics will be a combination of one- and two-track events, with the former being more frequent at low doses and the latter being much more frequent

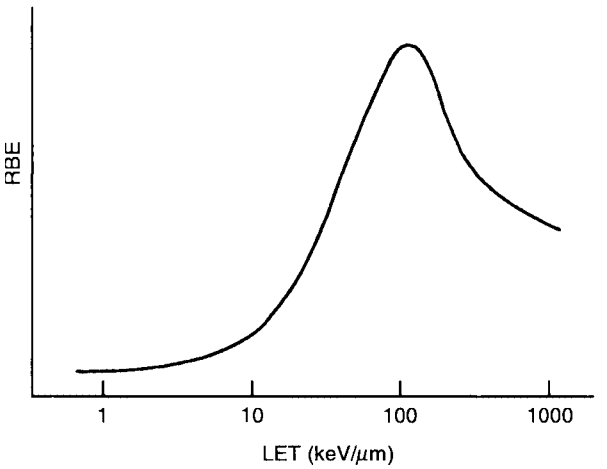

FIGURE 1.2 Generalized relationship between RBE and LET.

at high doses. The dose-response curve is generally assumed to fit the equation

$$Y = \alpha D + \beta D^2 \qquad (1.67)$$

where Y is the yield of dicentrics, D is the dose, α is the linear coefficient, and β is the dose-squared coefficient.

The dose-response curve for low LET radiation (X-rays or γ-rays) will be non-linear and best fit a linear-quadratic model. The dose-response curve for high LET radiation (for example, neutrons, protons, and α-particles) will be linear, or close to linear. RBE increases with increasing LET to a maximum of 100 keV/μm and decreases at higher LET values as a result of overkill.

Figure 1.3 shows a selection of dose-response curves.

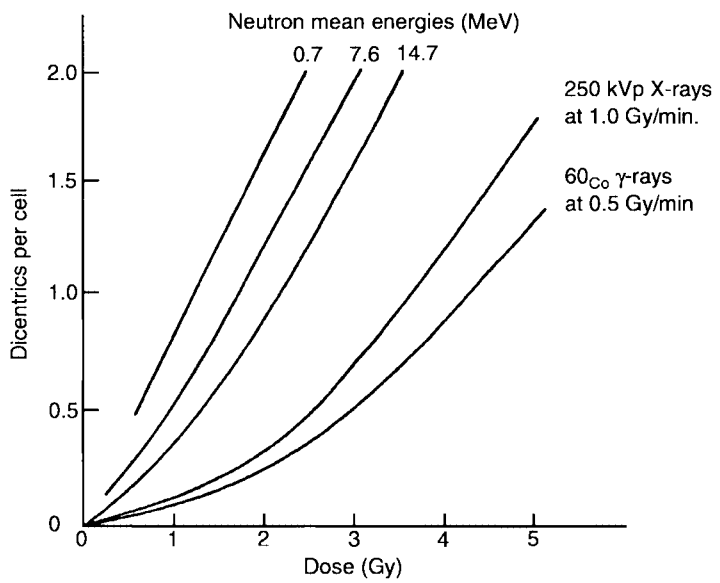

FIGURE 1.3 The relationship between dicentric yield and acute exposure to several types of radiation.

IX. CAVITY THEORY

The dose absorbed in different regions of an inhomogeneous medium is related to the stopping power of the material in the particular region. If the activity is the same and the radiation energy is the same, then the ratio of the doses in the different regions is the reciprocal of the stopping power in these regions. (Most of the investigation and theory was done for X- and γ-rays, which are the actual stopping power of electrons.)

If the cavity is small, most of the electrons are produced in the surrounding material, and the insertion of the cavity to the material does not change the electron spectrum. Bragg-Gray theory [10,11] is based on this assumption. It states that the energy lost by the electrons per unit volume in the cavity is $1/S$ times the energy lost by the gamma ray per unit volume in the solid. S is the stopping-power ratio in the gas and in the solid.

If the energy lost by electrons in crossing a volume is equal to the energy absorbed within the volume, then by the principle above the energy absorbed per unit volume in the gas is $1/S$ times the energy absorbed per unit volume of the solid. The energy absorbed in the gas is JW, where J is the ionization per unit volume of the gas (number of ion pairs produced) and W is the energy dissipated in ion-pair production. The Bragg-Gray relation states that the energy E_s absorbed per unit volume of the solid is

$$E_s = SW_sJ \tag{1.68}$$

By dividing the stopping power by the density, S_m, E_m, and J_m are the same quantities per unit mass:

$$S_m = \frac{\left(\frac{1}{\rho}\frac{dT}{dx}\right)_{solid}}{\left(\frac{1}{\rho}\frac{dT}{dx}\right)_{gas}} \tag{1.69}$$

If the energy lost in an ion pair production, W, is independent of energy, Laurence [12] derived the expression for ionization in the gas cavity:

$$J = K\int_0^{T_{max}} \lambda \int_0^{T_0} \frac{(dT/dx)_g}{(dT/dx)_s} dT\, dT_0 \tag{1.70}$$

where K is a constant and λ is the rate of electron production in the wall material per cm^3 per gamma ray. T_{max} is the highest electron energy in the initial spectrum. Spencer and Attix [13] and Burch [14] developed theories in which the secondary electrons were taken into account. In Spencer-Attix theory, a certain energy Δ was fixed, below which secondary electrons were assumed to dissipate all their energy at the site of interaction. Secondary electrons with energy above Δ were included in the fast spectrum. The lower energy limit of energy deposited in the gas was Δ. Spencer and Attix derived an expression for S_m by deriving an expression for the ratio of total to primary electron spectrum and using the Spencer-Fano [15] primary electron spectrum.

In Burch's theory the energy dissipated in the cavity per unit distance is defined as $(dT/dX)_g$ and the ratio of mass energy dissipation in the gas and in the solid $R_{m,T}$ is averaged:

$$\bar{R}_m = \frac{\int_0^{T_{max}} R_{m,T} n_{T,g} l_{T,g} \left(\frac{dT}{dx}\right)_g' dT}{\int_0^{T_{max}} n_{T,g} l_{T,g} \left(\frac{dT}{dx}\right)_g' dT} \tag{1.71}$$

where $n_{T,g}$ is the number of electrons crossing the cavity, $l_{T,g}$ is the average path length traversed in the gas, and the product $n_{T,g}\, l_{T,g}\, (dT/dX)_g'$ is the electron energy dissipated in the cavity by $n_{T,g}dT$ electrons.

Secondary-electron equilibrium at a point inside a material exists when the quotient

$$\frac{W_{in}^e - W_{out}^e}{\Delta m} \tag{1.72}$$

disappears for $\Delta m \to 0$. Here W_{in}^e is the sum of the kinetic energies of secondary electrons produced by photon radiation that enter a volume element ΔV containing the point; W_{out}^e is the sum of the kinetic energies of the secondary electrons that leave the volume element; and $\Delta m = \rho \Delta V$ is the mass of the material of density ρ within this volume element. This condition means that the absorbed dose produced at the point of interest is determined solely by the energy balance of the photon radiation entering and leaving the volume element, since the secondary-electron components of the energy balance counterbalance each other. For that reason the ratio of the absorbed doses produced by the same photon fluence at secondary-electron equilibrium in two different substances is equal to the ratio of the mass energy absorption coefficients.

REFERENCES

1. ***Radiation Quantities and Units***, ICRU Report 10a, published as National Bureau of Standards (U.S.) Handbook 84, 1962.
2. **Iwanami, S. and Oda, N.**, *Phys. Med. Biol.*, 44, 873, 1999.
3. ***Radiation Quantities and Units***, ICRU Report 16, 1970.
4. **Rossi, H. H.**, *Rad. Res.*, 10, 532, 1959.
5. ***Radiation Quantities and Units***, ICRU Report 33, 1980.

6. ***Quantities and Units in Radiation Protection Dosimetry,*** ICRU Report 51, 1993.
7. **Loevinger, R.,** *Radiology,* 62, 74, 1954; 66, 55, 1956.
8. **Fitzgerald, J. J. et al.,** *Mathematical Theory and Radiation Dosimetry,* Gordon & Breach, New York, 1967.
9. **ICRP Report 26,** Pergamon Press, New York, 1977.
10. **Bragg, W. H.,** *Phil. Mag.,* 20, 385, 1910.
11. **Gray, L. H.,** *Proc. Roy. Soc.,* A122, 647, 1929; A156, 578, 1936.
12. **Laurence, G. C.,** *Can. J. Res.,* A15, 67, 1937.
13. **Spencer, L. V. and Attix, F. H.,** *Rad. Res.,* 3, 239, 1955.
14. **Burch, P. R. J.,** *Rad. Res.,* 4, 361, 1955; 6, 79, 1957.
15. **Spencer, L. V. and Fano, U.,** *Phys. Rev.,* 93, 1172, 1954.

Taylor & Francis
Taylor & Francis Group
http://taylorandfrancis.com

2 Theoretical Aspects of Radiation Dosimetry

CONTENTS

I. Introduction 13
II. Electron Dosimetry 14
III. Photons Dosimetry 28
IV. Stopping Power 40
V. Energy for Ion Pair Production 44
VI. Electron Backscattering 46
VII. Dosimeter Perturbation 52
VIII. Dosimetry for Brachytherapy 56
IX. Proton Dosimetry 64
X. Cavity Theory 72
XI. Elements of Microdosimetry 77
References 82

I. INTRODUCTION

As the field of radiation dosimetry progressed, in particular for medical purposes, better equipment for more accurate dose measurement was developed. At the same time, theoretical methods for dose calculations and for calculation of correction factors of the various parameters affecting to dosimetry were developed.

Radiation therapy requires that a high dose of radiation is delivered accurately to specific organs. The success or failure of radiation treatment depends on the accuracy of the dose delivered to the tumor. Calibration of the radiation beam is based on complicated measurements and must be supported by accurate calculations and correction factors. Codes of practice were developed to guide medical physicists and physicians toward accurate dose delivery. High-energy electron beams are not monoenergetic but have a certain energy spread. This spread must be taken into consideration when the dose is measured and calculated. The energy spread has an effect on the electron range in the irradiated body. The most probable electron energy in the beam can be calculated. The range is generally obtained by the Harder equation, in which the electron energy is the main parameter.

Photon energy is well known if Cs^{137} and Co^{60} sources are used. When an accelerator is used to produce photons, the spectrum is *bremsstrahlung*, produced by the interaction of an electron beam with a target material. A set of parameters is then used to describe the beam spectrum. The advantage of using a photon beam is that its energy does not change with depth. Low-energy x-rays are generally characterized by the half-value layer (HVL)—the thickness of an absorber which reduces the beam intensity (or its air kerma) to 50% of its value before the attenuation. Aluminum is generally used for x-ray energy below 100 kV and copper is used above 100kV, and there is an overlap energy range below 100 keV.

Before any application of the radiation beam and the dosimeter is done, both beam and dosimeter must calibrated. For the beam calibration an air kerma must be established. The air kerma corresponds to the absorbed dose in air inside the dosimeter chamber cavity. The dosimeter calibration is given by the ratio of the dose to its cavity and the meter reading. These calibrations should be done both at the calibration beam and at the users beam. Following these steps, a series of corrections must be carried out in order to obtain the accurate dose for the patient. Since calibration is generally done in a water phantom, Bragg-Gray theory is used to make the transfer: dose to the cavity—dose to water—dose to patient. Dose correction must be done because of perturbation due to water displacement by the chamber, absorption and scattering in the chamber wall, and the fact that at least three different materials are involved. Energy per ion pair production must be known. The effective location of dose measurement, temperature, and pressure in the chamber must all be taken into consideration for accurate dose evaluation. In this chapter, methods used to calculate these corrections and theoretical ways to obtain an accurate value for the dose are discussed.

Analytical treatments generally begin with a set of coupled integro-differential equations that are prohibitively difficult to solve except under severe approximation. One such approximation uses asymptotic formulas to describe pair production and *bremsstrahlung*, and all other processes are ignored.

The Monte Carlo technique obviously provides a much better way for solving the shower generation problem, not only because all of the fundamental processes can be included, but also because arbitrary geometries can be treated. In addition, other minor processes, such as photoneutron production, can be added as a further generalization.

The most commonly used code for Monte Carlo calculation for dosimetry is the Electron-Gamma Shower (EGS) code. [1] The EGS system of computer codes is a general-purpose package for the Monte Carlo simulation of the coupled transport of electrons and photons in an arbitrary geometry for particles with energies above a few keV up to several TeV. The radiation transport of electrons (+ or −) or photons can be simulated in any element, compound, or mixture. That is, the data preparation package, PEGS4, creates data to be used by EGS4, using cross-section tables for elements 1 through 100. Both photons and charged particles are transported randomly rather than in discrete steps. The following physics processes are taken into account by the EGS4 Code System:

- *Bremsstrahlung* production (excluding the Elwert correction at low energies)
- Positron annihilation in flight and at rest (the annihilation quanta are followed to completion)
- Moliere multiple scattering (i.e., Coulomb scattering from nuclei)
- The reduced angle is sampled from a continuous, rather then discrete, distribution. This is done for arbitrary step sizes, selected randomly, provided that they are not so large or so small as to invalidate the theory.
- Moller ($e^- e^-$) and Bhabha (e^+e^-) scattering
- Exact, rather than asymptotic, formulas are used.
- Continuous energy loss applied to charged particle tracks between discrete interactions
- Pair production
- Compton scattering
- Coherent (Rayleigh) scattering can be included by means of an option
- Photoelectric effect.

II. ELECTRON DOSIMETRY

Electrons, as they traverse matter, lose energy by two basic processes: collision and radiation. The collision process is one whereby either the atom is left in an excited state or it is ionized. Most of the time the ejected electron, as in the case of ionization, has a small amount of energy that is deposited locally. On occasion, however, an orbital electron is given a significant amount of kinetic energy such that it is regarded as a secondary particle called a delta-ray. Energy loss by radiation (*bremsstrahlung*) is fairly uniformly distributed among secondary photons of all energies from zero up to the energy of the primary particle itself. At low-electron energies the collision loss mechanism dominates, and at high energies the *bremsstrahlung* process is the most important. At some electron energy the two losses are equal, and this energy coincides approximately with the critical energy of the material, a parameter that is used in shower theory for scaling purposes. Therefore, at high energies a large fraction of the electron energy is spent in the production of high-energy photons that, in turn, may interact in the medium. One of three photoprocesses dominates, depending on the energy of the photon and the nature of the medium. At high energies, an electron-positron-pair production dominates over Compton scattering, and at some lower energy the reverse is true. The two processes provide a return of energy to the system in the form of electrons which, with repetition of the *bremsstrahlung* process, results in a multiplicative process known as an electromagnetic cascade shower. The third photon process, the photoelectric effect, as well as multiple Coulomb scattering of the electrons by atoms, perturbs the shower to some degree. The latter, coupled with the Compton process, gives rise to a lateral spread. The net effect in the forward (longitudinal) direction is an increase in the number of particles and a decrease in their average energy at each step in the process.

Electron linac fields are usually characterized by the central-axis practical range in water, R_p, and the depth of half-maximum dose, R_{50}, for dosimetry, quality assurance, and treatment planning. The spectral quantity $\langle E_0 \rangle^*$ is introduced, defined as the mean energy of the incident spectral peak and termed the "peak mean energy." An analytical model was constructed by Deasy et al. [2] to demonstrate the predicted relation between polyenergetic spectral shapes and the resulting depth-dose curves. The model shows that, in the absence of electrons at the patient plane with energies outside about $\langle E_0 \rangle^* \pm 0.1 \langle E_0 \rangle^*$, R_p and R_{50} are both determined by $\langle E_0 \rangle^*$.

The two most common range-energy formulas currently used for clinical dosimetry are

$$\langle E_0 \rangle = 2.33 R_{50} \quad \text{MeV} \tag{2.1}$$

and

$$E_{p,0} = (0.22 + 1.98 R_p + 0.0025 R_p^2) \quad \text{MeV} \tag{2.2}$$

where E_0 denotes the energy at the patient plane (typically 100 cm from the source), $\langle E_0 \rangle$ is the mean energy,

$E_{p,0}$ is the most-probable energy of the incident beam, and the range parameters are measured in cm. These formulas imply that R_{50} is determined by the mean energy, whereas R_p is determined by the most-probable energy.

The mathematical technique used here is to relate the dose and dose gradient at depth s to the depth R_p for monoenergetic beams. These relations are then expressed as spectra-averaged quantities. We first write, for s in the linear falloff region,

$$D(s) + (R_p - s)\left(\frac{\partial D(z)}{\partial z}\right)_s = 0 \tag{2.3}$$

where $D(z)$ is the dose at depth z. Note that Equation (2.3) could be said to define R_p. If $\Phi_0(E_0)$ is defined as the fluence spectrum of electrons at the entrance plane (not the fluence spectrum at depth) and $dE_0 G(z, E_0)$ is defined as the central-axis depth-dose contribution at depth z from electrons of energies between E_0 and $E_0 + dE_0$. That is, $G(z, E_0)$ are depth-dose curves for monoenergetic beams. Also assume that $G(z, E_0)$ all have nearly a common maximum at the polyenergetic beam's depth of maximum dose (d_{max}). The expressions

$$D(z) = \int_{\Delta E} dE_0 \Phi_0(E_0) G(z, E_0) \tag{2.4}$$

and

$$\left(\frac{\partial D(z)}{\partial z}\right)_s = \int_{\Delta E} dE_0 \Phi_0(E_0)\left(\frac{\partial G(z, E_0)}{\partial z}\right)_s \tag{2.5}$$

follow. Consistent with the assumption of negligible low-energy contamination, the integrals are taken over only the peak energy region, denoted by ΔE. Equation (2.5) follows since these are definite, well-behaved integrals of well-behaved functions.

An electron-beam dose calculation algorithm has been developed by Keall and Hoban [3] which is based on a superposition of pregenerated Monte Carlo electron track kernels. Electrons are transported through media of varying density and atomic number using electron tracks produced in water. The perturbation of the electron fluence due to each material encountered by the electrons is explicitly accounted for by considering the effect of varying stopping power, scattering power, and radiation yield.

To accurately transport charged particles through a heterogeneous absorbing medium, knowledge of these three parameters of the different components in the medium is required. For an absorbing medium of density ρ, ICRU Report 35 gives the expression for scattering power T as

$$T = \pi\rho\left(\frac{2r_e Z}{(\tau+1)\beta^2}\right)^2 \times \frac{N_A}{M_A}\left[\ln\left(1+\left(\frac{\theta_m}{\theta_\mu}\right)^2\right) - 1 + \left(1+\left(\frac{\theta_m}{\theta_\mu}\right)^2\right)^{-1}\right] \tag{2.6}$$

where r_e is the classical electron radius, $\tau = E/m_e c^2$ is the ratio of the kinetic energy E of the electrons to the rest energy (the rest energy equals the rest mass, m_e, times the speed of light squared, c^2), β is the ratio of the velocity of the electron to c, N_A is Avagadro's constant, M_A is the molar mass of substance A, θ_m is the cutoff angle due to the finite size of the nucleus, and θ_μ is the screening angle. The collision stopping power S_{col} can be calculated from

$$S_{col} = \frac{2\pi\rho r_e^2 m_e c^2 N_A Z}{\beta^2 M_A}\left[\ln\left(\frac{\tau^2(\tau+2)}{2(I/m_e c^2)^2}\right) + F(\tau) - \delta\right] \tag{2.7}$$

where I is the mean excitation energy, δ is the density effect correction, and

$$F(\tau) = 1 - \beta^2 + \left[\tau^2/8 - (2\tau+1)\ln 2\right]/(\tau+1)^2 \tag{2.8}$$

For an incident kinetic energy E_0 and radiative stopping power S_{rad}, ICRU 37 uses the following equation to calculate the radiation yield, $Y(E_0)$:

$$Y(E_0) = \frac{1}{E_0}\int_0^{E_0} \frac{S_{rad}(E)}{S_{col}(E) + S_{rad}(E)}\, dE \tag{2.9}$$

In the Super Monte Carlo (SMC) method, the above equations are used to translate electron transport in water to electron transport in a medium of arbitrary composition.

SMC electron dose distributions are calculated by superimposing the dose contribution from the electron track kernel, which is initiated from every surface voxel within the treatment field. At each surface voxel, the dose from the kernel is determined by transporting each electron step of each electron track. The dose is found by summing the energy deposited in voxel i, j, k from electron track which fall in voxel i, j, k, from all of the tracks

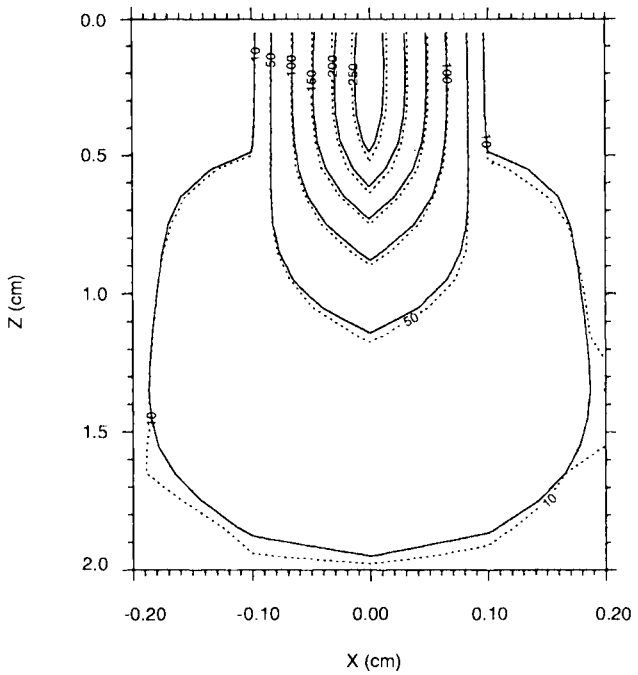

FIGURE 2.1 The dose distributions resulting from a 15-MeV pencil beam incident on a water phantom calculated using Monte Carlo (—) and SMC (---). The numbers on the isodose curves represent dose per incident fluence (pGy cm^2). (From Reference [3]. With permission.)

transported from the surface in field *XY*.

$$D(i,j,k) = \frac{1}{\rho_{i,j,k}} \sum_{XY} \left(\sum_{m=0}^{M} \sum_{l=q}^{q'} \Delta E_{dep,m,l} \right) \qquad (2.10)$$

q, q' are steps in the calculation and m denotes an electron track.

The SMC algorithm can also be used to calculate dose by only taking account of the density of the irradiated medium and not the composition. This option is performed by transporting the electron step by its original length, divided by the density of the irradiated medium, instead of taking full account of the stopping power and scattering power characteristics of the medium. This option saves computation time and is useful when only waterlike media (e.g., soft tissue) are irradiated.

Isodose curves for a 15-MeV pencil beam were calculated using SMC and Monte Carlo methods in a water phantom with $0.1 \times 0.1 \times 0.1$ cm^{-3} voxels. The results are shown in Figure 2.1. Agreement is obtained between the SMC and Monte Carlo dose distributions, as expected, because the electron track kernel is generated in water. Figure 2.1 shows that 3000 electrons give a smooth dose distribution for all but the lowest isodose level and, hence, the neglect of *bremsstrahlung* transport in the SMC calculation is valid. The maximum difference found between the dose in any two corresponding voxels in the dose distribution was 5% of the maximum dose in the distributions.

The Method of Moments was generalized by Larsen et al. [4] to predict the dose deposited by a prescribed source of electrons in a homogeneous medium. The essence of this method is first to determine, directly from the linear Boltzmann equation, the exact mean fluence, mean spatial displacements, and mean-squared spatial displacements as functions of energy, and second to represent the fluence and dose distributions accurately using this information. Unlike the Fermi-Eyges theory, the Method of Moments is not limited to small-angle scattering and small angle of flight, nor does it require that all electrons at any specified depth z have one specified energy $E(z)$. The sole approximation in the Larsen et al. application is that for each electron energy E, the scalar fluence is represented as a spatial Gaussian, whose moments agree with those of the linear Boltzmann solution.

The mean particle motion is along the z-axis. As E decreases from E_0 to 0, $z(E)$ increases from 0 to a finite value, which is less than the electron range unless $T = 0$. Individual electrons may increasingly stray from this mean position as E decreases. Therefore, the variances in particle positions should all increase as E decreases.

Figure 2.2 shows the broad-beam depth doses for the MM-BCSD (BCSD ≡ Boltzmann Continuous Slowing Down), MM-FP (FP ≡ Fokker Planck), and EGS4 simulations. The shapes of the two MM simulations are globally correct. The differences between the Monte Carlo and the MM-BCSD results are due to the assumption of a spatial Gaussian, while the differences between the

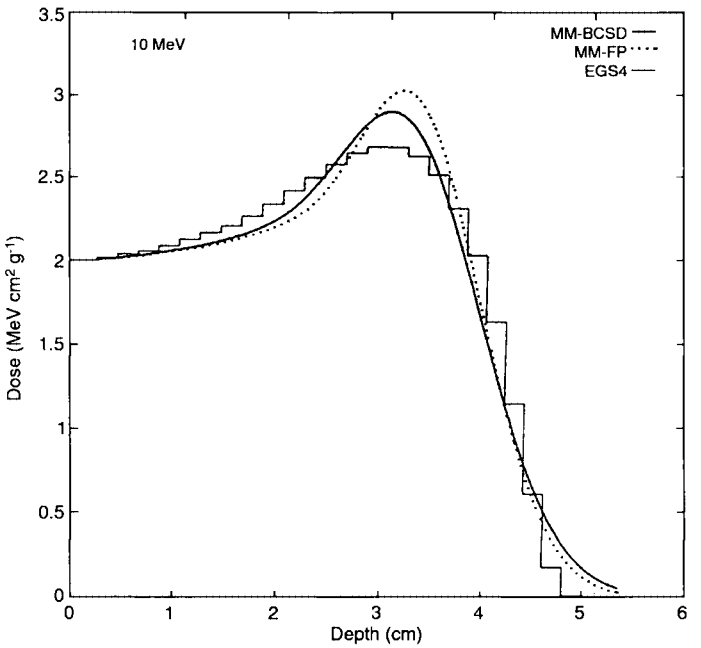

FIGURE 2.2 Depth dose curve for a broad 10-MeV electron beam. (From Reference [4]. With permission.)

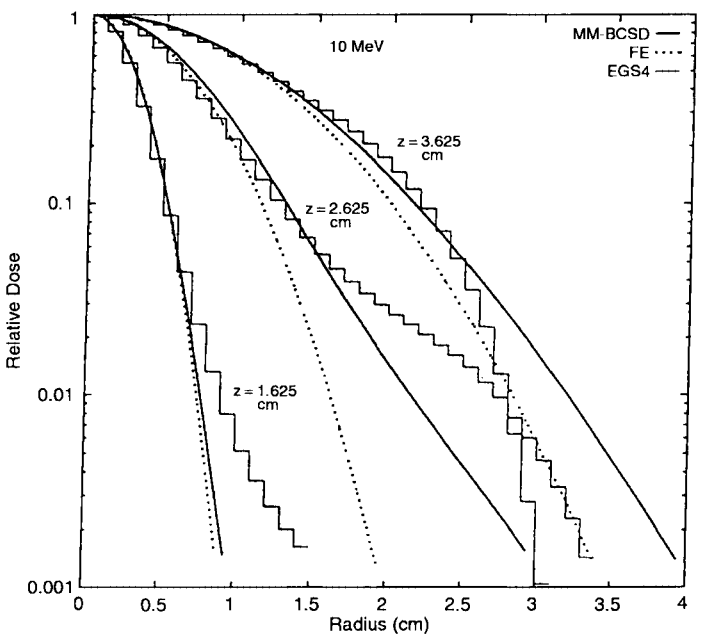

FIGURE 2.3 Radial dose profiles for a 10-MeV electron pencil beam. (From Reference [4]. With permission.)

Monte Carlo and the MM-FP results are due to the spatial Gaussian assumption and the small angle of scattering approximation. For these problems, the omission of large-angle scattering in the MM-FP simulation leads to an error in the depth-dose distribution that is approximately double that of the MM-BCSD simulation. [4]

In Figure 2.3 radial dose profiles are plotted from the MM-BCSD, Fermi-Eyges, and EGS4 simulations at different depths. Near the central axis, the MM-BCSD and Fermi-Eyges profiles are remarkably similar. Away from the central axis, the MM-BCSD results are consistently greater than the Fermi-Eyges results and agree with the Monte Carlo results over a larger range. The MM-FP profiles are very similar to the other profiles near the central axis; away from the central axis, they are closer to the MM-BCSD results than to the Fermi-Eyges results.

Dose in water at a depth d_{water} is related to the dose in a solid at a corresponding depth d_{med}, provided secondary

electron equilibrium exists (normally within a few mm of the surface) and energy spectra at each position are identical [9], by

$$D_{water}(d_{water}) = D_{med}(d_{med})[(S/\rho)_{coll}]_{med}^{water}[\Phi]_{med}^{water} \tag{2.11}$$

where $[(\bar{S}/\rho)_{col}]_{med}^{water}$ is the ratio of the mean unrestricted mass collision stopping power in water to that in the solid. $[\Phi]_{med}^{water}$ is the fluence factor, that is, the ratio of the electron fluence in water to that in the solid phantom. Because energy-loss straggling and multiple scattering depend upon the effective atomic number of the phantoms, it is not possible to find corresponding depths where the energy spectra are identical. However, there are corresponding depths where the mean energies are identical. Equation (2.12) is assumed to hold for these depths, which are defined to be the equivalent depths.

It is recommended that the water-equivalent depth be approximated using a density determined from the ratio of R_{50} penetrations by

$$d_{water} = d_{med} \times \rho_{eff} = d_{med}\left(\frac{R_{50}^{water}}{R_{50}^{med}}\right) \tag{2.12}$$

i.e., that the effective density be given by the ratio of the R_{50} in water to that in the non-water material.

In order for Equation (2.11) to apply, secondary electron equilibrium must hold, which requires that the detector be of minimal mass or be made of material identical to the phantom. Therefore, it is recommended that thick-walled ion chambers (>0.1 g/cm^2) be irradiated in phantoms made of the same material. For example, the Memorial Holt parallel-plate chamber should be used in clear polystyrene and the PTW Markus parallel-plate chamber in PMMA. Thin-walled ion chambers, e.g., the graphite-walled Farmer chamber, can be used in any of the solid phantoms. In the measurement of depth dose, the conversion of ionization to dose is given by Andreo et al. [65]:

$$D_{water}(d_{water}) = N_{gas}Q_{corr}(d_{med})[(\bar{L}/\rho)_{coll}]_{air}^{med}P_{repl} \times [(\bar{S}/\rho)_{coll}]_{med}^{water}[\Phi]_{med}^{water} \tag{2.13}$$

where $Q_{corr}(d_{med})$ is the corrected ionization reading; $[(\bar{L}/\rho)_{coll}]_{air}^{med}$ is the ratio of the mean restricted mass collision stopping power in water to that in air. Percent depth dose is then given by

$$\%D_{water}(d_{water}) = \left(\frac{\{Q_{corr}(d_{med}) \times [(\bar{L}/\rho)_{coll}]_{air}^{water} \times [\Phi]_{med}^{water} \times P_{repl}\}}{[\ldots]_{max}}\right) \times 100 \tag{2.14}$$

where the denominator equals the value of the numerator at the depth-of-maximum dose.

In radiation dosimetry protocols, plastic is allowed as a phantom material for the determination of absorbed dose to water in electron beams. The electron fluence correction factor is needed in conversion of dose measured in plastic to dose in water. There are large discrepancies among recommended values as well as measured values of electron fluence correction factors when polystyrene is used as a phantom material. Using the Monte Carlo technique, Ding et al. [5] have calculated electron fluence correction factors for incident clinical beam energies between 5 and 50 MeV as a function of depth for clear polystyrene, white polystyrene, and PMMA phantom materials.

The dose to water at dose maximum in a water phantom, D_w^w is related to the dose to plastic at dose maximum in a plastic phantom, D_p^p, by

$$D_w^w(d_{max}^w) = D_p^p(d_{max}^p)\left(\frac{\bar{S}}{\rho}\right)_p^w \phi_p^w \quad \text{Gy} \tag{2.15}$$

where $(S/\rho)_p^w$, is the Bragg-Gray ratio of the mean unrestricted mass collision stopping power in water to that in the solid and ϕ_p^w is the electron fluence correction factor defined above. (D_B^A refers to the dose to medium B in a phantom of medium A.) The TG-21 protocol takes $(S/\rho)_p^w$ to be constant with respect to beam energy, with a value of 1.03 for polystyrene and 1.033 for PMMA. It also takes $\phi_{PMMA}^w = 1.0$ for all energies and tabulates $\phi_{polystyrene}^w$ vs. the beam's mean energy on the surface (ranging from 1.039 at 5 MeV to 1.009 at 16 MeV).

The AAPM TG-25 protocol's approach is similar to that of TG-21 except for the dose to water in a water phantom, D_w^w is related to the dose to plastic in a plastic phantom, D_p^p, for arbitrary scaled depths rather than just d_{max}. The relationship is given by:

$$D_w^w(d^w) = D_p^p(d^p)\left(\frac{\bar{S}}{\rho}\right)_p^w \phi_p^w \quad \text{Gy} \tag{2.16}$$

where the depth in water (in cm), d^w, is related to the depth in plastic, d^p, by a depth-scaling factor called the effective density ρ_{eff}:

$$d^w = d^p\rho_{eff} = d^p\frac{R_{50}^w}{R_{50}^p} \quad \text{cm} \tag{2.17}$$

where R_{50}^w and R_{50}^p are the depths (in cm) at which the absorbed dose falls to 50% of its maximum in water and plastic, respectively.

In the AAPM TG-21 protocol, which is based on Spencer-Attix cavity theory, the dose to a medium in a

phantom of that medium is given by:

$$D_{med}^{med}(d^{med}) = M^{med}(d^{med})N_{gas}\left(\frac{\bar{L}}{\rho}\right)_a^{med} \times (P_{ion}P_{repl}P_{wall})^{med} \text{ Gy} \quad (2.18)$$

where $M^{med}(d^{med})$ is the ion chamber meter reading measured in the medium. d^{med} is the depth of the measurement. $[\bar{L}/\rho]_a^{med}$ is the ratio of the mean restricted mass collision stopping power in the medium to that in air and the P corrections are defined by the AAPM TG-21 protocol and are in principle, dependent on the medium of the phantom. Combining Equation (2.16) and Equation (2.18) gives TG-25's estimate of the dose to water, given a measurement at the scaled depth in a plastic phantom:

$$D_w^w(d^w) = M^p(d^p)N_{gas}\left(\frac{\bar{L}}{\rho}\right)_a^p \times (P_{ion}P_{repl}P_{wall})^p\left(\frac{\bar{S}}{\rho}\right)_p^w \phi_p^w \text{ Gy} \quad (2.19)$$

The IAEA TR277 Code of Practice and the NACP protocol have a definition of electron fluence correction factor which is different from that of the AAPM protocols. The IAEA converts the electrometer reading at the ionization maximum in a plastic phantom to the equivalent reading at the ionization maximum in a water phantom using

$$M_u^w = M_u^p h_m \quad C \quad (2.20)$$

where M_u^w and M_u^p are the electrometer readings in water and plastic, respectively, corrected for ion recombination by P_{ion}:D_w^w.

The IAEA gives the absorbed dose to water in a water phantom, D_w^w, at the effective point of measurement by:

$$D_w^w(P_{eff}) = M_u^w N_{gas}\left(\frac{\bar{L}}{\rho}\right)_{air}^w (P_{wall}P_{fl})^w \text{ Gy} \quad (2.21)$$

where in the IAEA notation, $[\bar{L}/\rho]_{air}^w$ is written as $(S_{w,air})_u$, N_{gas} as N_D, $P_{fl}P_{wall}$ as p_u, and P_{eff} is the effective point of measurement.

The overall IAEA equation for assigning dose to water based on a measurement in a plastic phantom is:

$$D_w^w(P_{eff}^w) = M_u^p(z_{max}^p)h_m N_{gas}\left(\frac{\bar{L}}{\rho}\right)_a^w (P_{wall}P_{fl})^w \text{ Gy} \quad (2.22)$$

where z_{max}^p is the depth of the maximum ionization in plastic and p_{eff}^w is at the depth of ionization maximum in the water phantom.

A more rigorous approach gives

$$\left(\frac{\bar{L}}{\rho}\right)_p^w \times \left(\frac{\bar{L}}{\rho}\right)_a^p = \left(\frac{\bar{L}}{\rho}\right)_a^w \quad (2.23)$$

which gives

$$D_w^w(d^w) = M^p(d^p)N_{gas}\left(\frac{\bar{L}}{\rho}\right)_a^w (P_{ion}P_{repl}P_{wall})^p\phi_p^w \text{ Gy} \quad (2.24)$$

where $M^p(d^p)$ is the ion chamber reading measured in a plastic phantom at depth d^p, corresponding to the scaled depth in water at which the dose is desired, and D_w^w is the dose to water in a water phantom. Equation (2.24) can be used to obtain the dose to water in a water phantom directly from the measurement performed in a plastic phantom.

Calculated central-axis depth-dose curves in different phantom materials with an identical incident beam are shown for two beams in Figure 2.4.

Figure 2.5 compares $(\bar{L}, \rho)_p^w$ to $(\bar{L}, \rho)_a^w/(\bar{L}, \rho)_a^p$ and shows that they agree within 0.2% up to the depth of R_{50}. This demonstrates that the depth-scaling procedure, which was defined to give equivalent depths at which mean energies match, also gives depths at which the entire electron spectra are effectively the same since the stopping-power ratios are close to identical. Figure 2.6 shows the calculated Spencer Attix water to plastic stopping power ratio for electron beams.

The accuracy of the Monte Carlo algorithm for fast electron dose calculation, VMC, was demonstrated by Fippel et al. [6], by comparing calculations with measurements performed by a working group of the National Cancer Institute (NCI) of the USA. For both energies investigated, 9 and 20 MeV, the measurements in water are taken to determine the energy spectra of the Varian Clinac 1800 accelerator. In some cases deviations have been observed which could be explained by the incompletely known geometry on the one hand and by inconsistent data on the other.

Most of the commercially available 3D electron beams planning systems use pencil-beam algorithms. Algorithms of this type may produce large errors (up to 20%) when small, dense inhomogeneities are present in an otherwise homogeneous medium. These errors are mainly caused by the semi-infinite-slab approximation of the patient geometry.

The VMC (Voxel Monte Carlo) algorithm can be briefly described as follows. To simulate the head of the accelerator for a definite energy, a fluence distribution in energy $F(E, \beta_0, x_0)$, denoted as the energy spectrum for short, at the phantom surface is necessary, with β_0 and x_0 being the initial direction and position and E being the kinetic energy of the primary electron. For simplicity, we assume that this spectrum is independent of β_0 and x_0; i.e.,

$$F(E, \beta_0, x_0) = F(E, 0, 0) \equiv F(E) \quad (2.25)$$

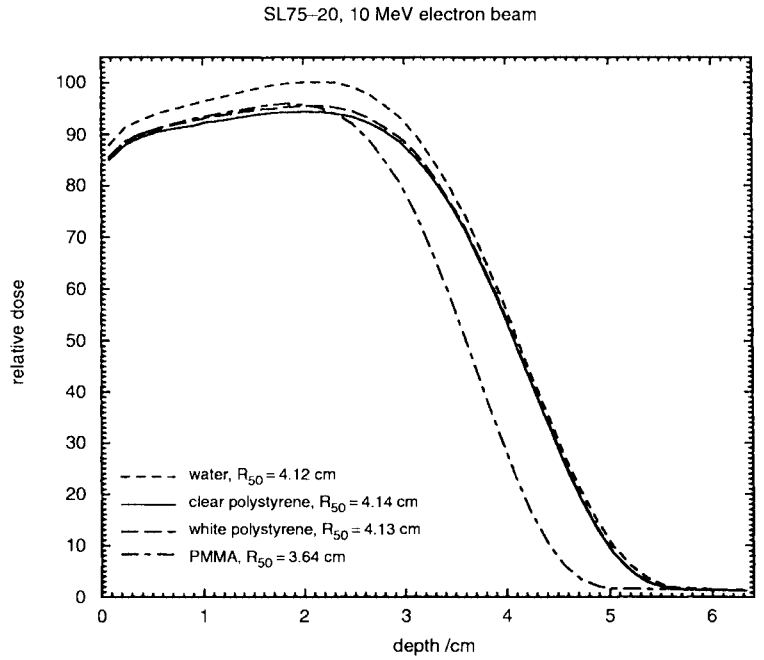
SL75-20, 10 MeV electron beam
relative dose
depth /cm
water, R50 = 4.12 cm
clear polystyrene, R50 = 4.14 cm
white polystyrene, R50 = 4.13 cm
PMMA, R50 = 3.64 cm

FIGURE 2.4 Calculated central-axis dose curves of a 10-MeV electron beam from an SL75-20 accelerator in different phantom materials. Curves all normalized to the maximum of the water curve (From Reference [5]. With permission.)

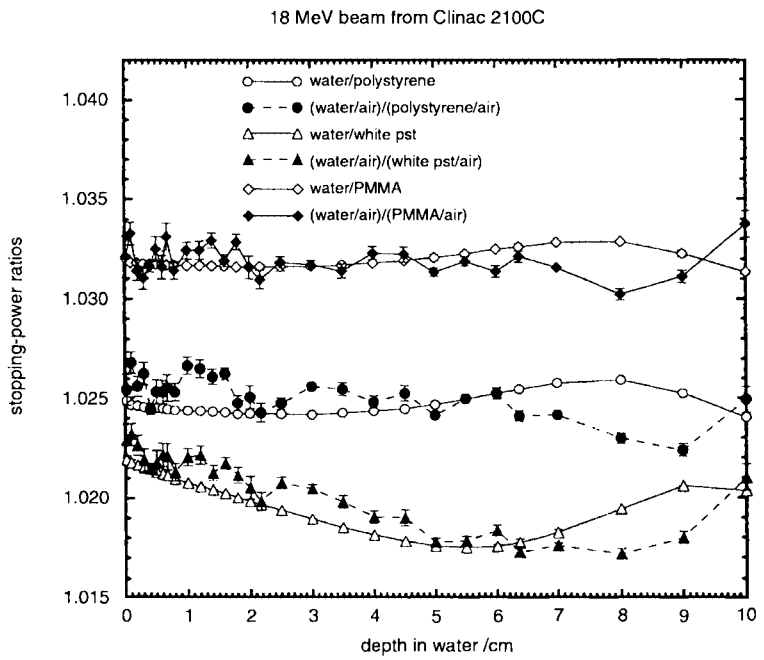

FIGURE 2.5 A comparison between calculated Spencer-Attix stopping-power ratios for an 18-MeV beam (R_{50} = 7.7 cm) from a Clinac 2100C. The empty symbols are the calculated $(\bar{L}, \rho)_p^w$ in water and the filled symbols are the calculated $(\bar{L}, \rho)_a^w$ in water divided by the calculated $(\bar{L}, \rho)_a^p$ in plastic where the depths in plastic are scaled to the water-equivalent depth according to Equation (2.17). This shows that $(\bar{L}, \rho)_p^w$ and $(\bar{L}, \rho)_a^w/(\bar{L}, \rho)_a^p$ agree within 0.2%, indicating that the depth-scaling procedure is giving equivalent depths at which the electron spectra are close to identical (From Reference [5]. With permission.)

If this spectrum, the depth dose of a monoenergetic broad beam in water $D_{mono}(E, z)$, and the photon background $D_\gamma(z)$ are known, then the depth-dose curve in water for the accelerator can be calculated by

$$D(z) = D_\gamma(z) + \int dE F(E) D_{mono}(E, z) \qquad (2.26)$$

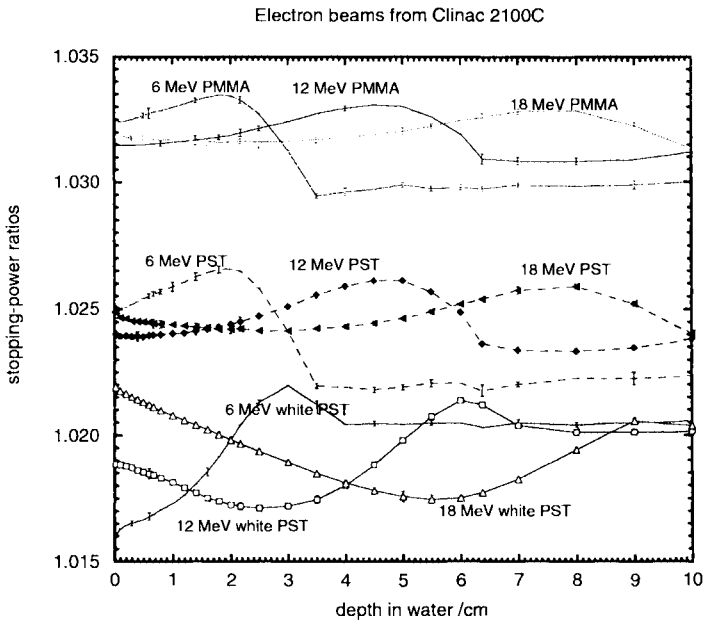

FIGURE 2.6 Calculated Spencer-Attix water to plastic stopping-power ratios for electron beams from the Clinac 2100C as a function of beam energy and depth for PMMA, clear and white polystyrene. The AAPM recommends using energy and depth independent values of 1.03 and 1.033 for polystyrene and PMMA, respectively. (From Reference [5]. With permission.)

Fippel et al. assumed

$$F(E) = C[A(2m + E) + 1/(E_x - E)^3]$$
$$E_{min} \leq E \leq E_p < E_x \tag{2.27}$$

Here, C is the normalization constant, $m = 0.511$ MeV is the electron mass, $E_{min} = 0.5$ MeV is the minimum energy, and A, E_x, and E_p are free parameters (E_p is the most probable energy and at the same time the maximum energy of the spectrum). To fit these parameters, they pre-calculated a set of curves $D_{mono}(E, z)$ in the energy range of 0.5 MeV $\leq E \leq$ 30 MeV for the large field size (15 cm $\times$ 15 cm) using VMC. From the measured depth-dose curves $D_{meas}(z)$ of the Varian Clinac 1800 accelerator in water, the gamma contribution $D_\gamma(z)$ is subtracted. Then, using Equation (2.26), $(D_{meas}(z) - D(z))^2$ is minimized and $F(E)$ is determined. Gauss-Legendre quadrature has been used to perform the integration in Equation (2.26).

Figure 2.7 shows percentage depth doses in water for SSD = 100 cm and SSD = 110 cm as calculated by VMC (with the spectra $F(E)$) and the MDAH (M.D. Anderson Hospital) algorithm compared to measurements. The base data for the pencil-beam algorithm have been created using the water measurements.

A new approach was proposed by Rogers et al. [7] for electron-beam dosimetry under reference conditions. The approach has the following features:

- It uses ion chambers and starts from an absorbed-dose calibration factor for ^{60}Co to be consistent with the present proposal for the new AAPM photon-beam protocol
- It uses R_{50} to specify the beam quality and the reference depth ($d_{ref} = 0.6R_{50} - 0.1$ [all quantities in cm])
- It has a formalism which is parallel to the k_Q formalism for photon-beam dosimetry
- It fully accounts for the impact on stopping-power ratios of realistic electron beams
- It allows an easy transition to using primary standards for absorbed dose to water in electron beams when these are available

The equation for dose to water under reference conditions is:

$$D_w^Q = MP_{ion}{}^{P_{gr}^Q} K'_{R50} K_{ecal} N_{D,w}^{^{60}\mathrm{Co}} \tag{2.28}$$

The term P_{gr}^Q is not needed with plane-parallel chambers but corrects for gradient effects with cylindrical chambers and is measured in the user's beam. The parameter k_{ecal} is associated with converting the ^{60}Co absorbed-dose calibration factor into one for an electron beam of quality Q_e and contains most of the chamber-to-chamber variation. The factor k'_{R50} is a function of R_{50} and converts the absorbed-dose calibration factor to that for the electron-beam equality of interest. Two analytical expressions were presented by Rogers that are close to universal expressions for all cylindrical Farmer-like chambers and for well-guarded plane-parallel chambers, respectively. [7]

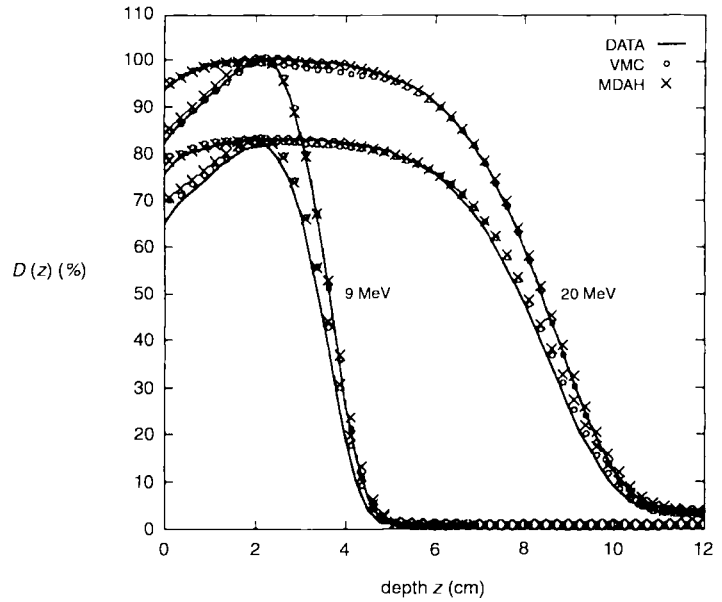

FIGURE 2.7 Depth dose curves in water as calculated by VMC and the MDAH algorithm, compared with measurements for SSD = 100 cm and SSD = 110 cm. (From Reference [6]. With permission.)

The fundamental equations of the k_Q formalism are

$$D_w^Q = MP_{ion}k_Q N_{D,w}^{Q_0} \quad \text{Gy} \tag{2.29}$$

$$N_{D,w}^Q = k_Q N_{D,w}^{Q_0} \tag{2.30}$$

where D_w^Q is the absorbed dose to water (in Gy) at the point of measurement of the ion chamber when it is absent (this is the center of a cylindrical or spherical chamber, or the front of the air cavity in a plane-parallel ion chamber); M is the temperature and pressure-corrected electrometer reading in coulombs (C) or meter units (rdg); P_{ion} accounts for ion chamber collection efficiency not being 100%; $N_{D,w}^{Q_0}$ is the absorbed dose to water calibration factor for an ion chamber placed under reference conditions in a beam of quality Q_0; $N_{D,w}^Q$ is the calibration factor in a beam of duality Q; and k_Q accounts for the variation in the calibration factor between beam quality Q and the reference beam quality Q_0. These equations can be applied to electron or photon beams. In practice, the reference beam quality Q_0 is ^{60}Co. The general equation for k_Q is

$$k_Q = \frac{\left[\left(\frac{\bar{L}}{\rho}\right)_{air}^{w} P_{wall}P_{fl}P_{gr}^Q P_{cel}\right]_Q}{\left[\left(\frac{\bar{L}}{\rho}\right)_{air}^{w} P_{wall}P_{fl}P_{gr}^Q P_{cel}\right]_{Q_0}} \tag{2.31}$$

where the numerator and denominator are evaluated for the beam quality Q of interest and the calibration beam quality Q_0, respectively. P_{cel} is a correction for the central electrode if it is made of a material different from the chamber walls. k_Q for electron beams has two components: $k_{R_{50}}$, which depends on the chamber but is a function only of the beam quality specifier R_{50}, and P_{gr}^Q, which extracts the gradient corrections and which, for a cylindrical chamber, depends on the shape of the particular depth-dose curve being measured; i.e.,

$$k_Q = P_{gr}^Q k_{R_{50}} \tag{2.32}$$

where

$$k_{R_{50}} = \frac{\left[\left(\frac{\bar{L}}{\rho}\right)_{air}^{w} P_{wall}P_{fl}P_{cel}\right]_{R_{50}}}{\left[\left(\frac{\bar{L}}{\rho}\right)_{air}^{w} P_{wall}P_{fl}P_{gr}^Q P_{cel}\right]_{^{60}\text{Co}}} \tag{2.33}$$

and

$$\begin{aligned} P_{gr}^Q &= I(d_{ref} + 0.5r_{cav})/I(d_{ref}) \\ &\quad \text{[for cylindrical chambers]} \\ &= 1.0 \quad \text{[for plane-parallel chambers]} \end{aligned} \tag{2.34}$$

where $I(d)$ is the ionization reading of a cylindrical chamber placed with the cylindrical axis at depth d and r_{cav} is the radius of the chamber's cavity in cm.

$$D_w^Q = MP_{ion}P_{gr}^Q k_{R_{50}} N_{D,w}^{^{60}\text{Co}} \quad \text{Gy} \tag{2.35}$$

The values of $k_{R_{50}}$ are calculable as a function of R_{50} and depend only on the chamber. For cylindrical chambers, the user must measure P_{gr}^Q in their own electron beam, but for plane-parallel chambers, $P_{gr}^Q = 1.0$ (see Figures 2.8, 2.9, 2.10, and 2.11).

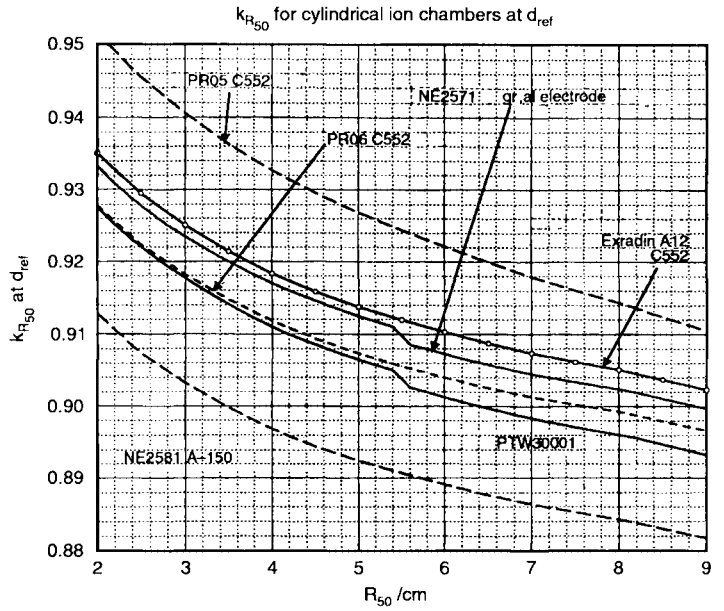

FIGURE 2.8 Calculated values of $k_{R_{50}}$ as a function of R_{50} for several common cylindrical ion chambers. These values can be used with a ^{60}Co absorbed-dose to water calibration factor to assign dose to water at the reference depth $d_{ref} = 0.6\ R_{50} - 0.1$ cm. (From Reference [7]. With permission.)

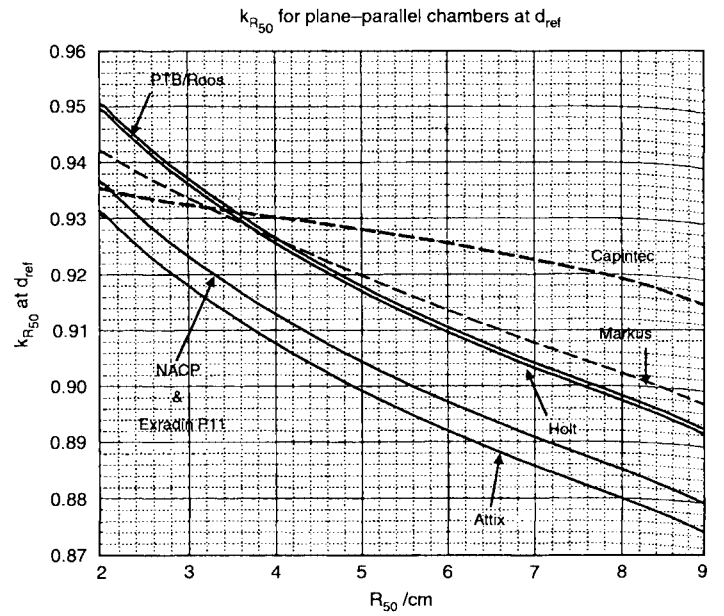

FIGURE 2.9 Calculated values of $k_{R_{50}}$ as a function of R_{50} for several common plane-parallel chambers. These values can be used with a ^{60}Co absorbed-dose to water calibration factor to assign dose to water at the reference depth $d_{ref} = 0.6R_{50} - 0.1$ cm. (From Reference [7]. With permission.)

Once electron-beam absorbed-dose calibration factors are available, one could use the following dose equation:

$$D_w^Q = MP_{ion}\frac{P_{gr}^Q}{P_{gr}^{Q_e}}k'_{R_{50}}N_{D,w}^{Q_e} \quad \text{[cylindrical chambers]} \tag{2.36}$$

$$= MP_{ion}k'_{R_{50}}N_{D,w}^{Q_e} \quad \text{[plane-parallel chambers]} \tag{2.37}$$

The major complication in this procedure is the need to measure P_{gr}^Q correction factors in the user's beam if d_{ref} cylindrical chambers are used.

The recommendations of the Electron Dosimetry Working Party II of the UK Institution of Physics and Engineering in Medicine and Biology [8], consist of a code of practice for electron dosimetry for radiotherapy beams of initial energy from 2 to 50 MeV. The code

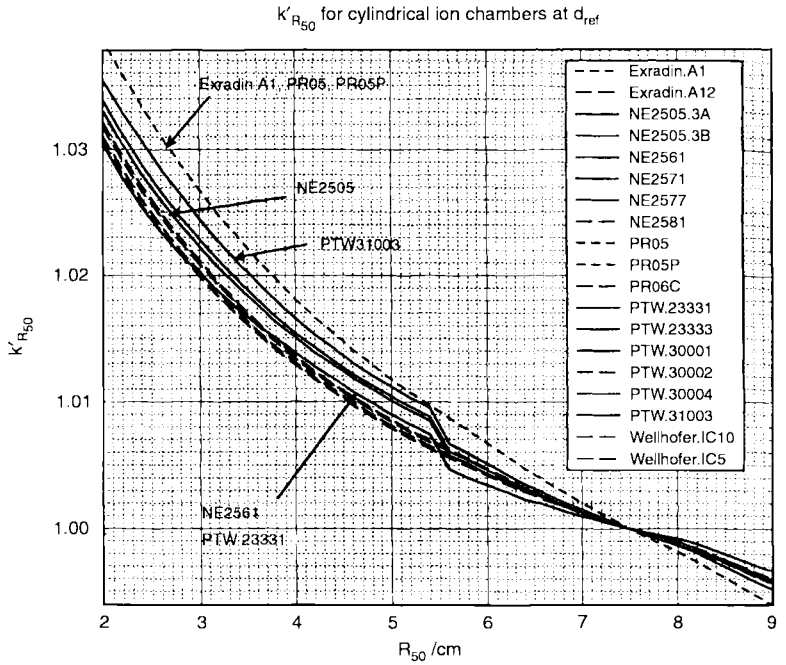

FIGURE 2.10 Calculated values of $k'_{R_{50}}$ as a function of R_{50} for cylindrical ion chambers. These values can be used with a ^{60}Co absorbed-dose to water calibration factor to assign dose to water at the reference depth $d_{ref} = 0.6R_{50} - 0.1$ cm. Note that chambers with aluminum lectodes are shown as solid lines. The upper two curves at smaller values or $k'_{R_{50}}$ represent curves which have cavity diameters less than 6 mm. (From Reference [7]. With permission.)

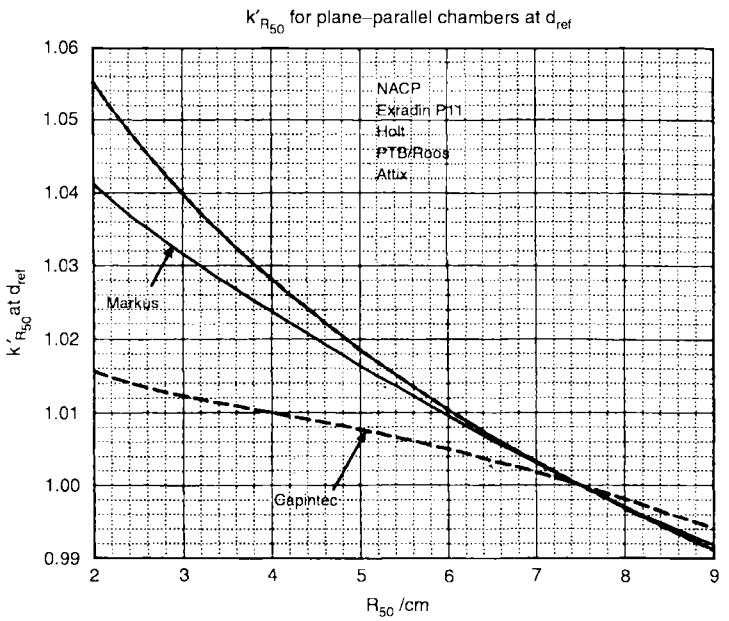

FIGURE 2.11 Calculated values of $k'_{R_{50}}$ as a function of R_{50} for several common plane-parallel chambers. These values can be used to determine absorbed-dose to water at the reference depth $d_{ref} = 0.6R_{50} - 0.1$ cm. Note that the values for the five well-guarded chambers lie on the same line in the figure. (From Reference [7]. With permission.)

is based on the 2 MV (or ^{60}Co) air kerma calibration of the NE 2561/2611 chamber, which is used as the transfer instrument between the national standards laboratory and hospitals in the UK. The code utilizes an $N_{D,air}$ approach. Designated chambers are the NE 2571 (graphite-walled Farmer chamber), to be calibrated against the transfer instrument in a megavoltage photon beam, and three parallel-plate chambers, to be

calibrated against the NE 2571 in a higher-energy electron beam.

The current approach to electron dosimetry (*code of practice*) changes the conceptual framework to one based on $N_{D,air}$, a traceable calibration factor for the electron chamber to convert its reading to mean dose to air in the sensitive volume under standard ambient conditions. This enables the calibration of parallel-plate electron chambers in an electron beam. The recommended calibration route retains the NPL-designed secondary-standard chamber as the transfer instrument link between that national standards laboratory and hospital. It also retains a 2 MV/^{60}Co air kerma calibration of the instrument as the basis of the calibration route. Graphite-walled Farmer chambers are still to be calibrated in the hospital against the secondary-standard chamber at 5 cm depth in a phantom in either a ^{60}Co gamma-ray beam or megavoltage x-ray beam, now in terms of $N_{D,air}$. Parallel-plate chambers are then to be calibrated, also in terms of $N_{D,air}$, against a previously calibrated graphite-walled Farmer chamber at a reference depth equal to or nearly equal to the depth of the dose maximum in a sufficiently high-energy electron beam. This is due to the relatively large reported variation in photon beam perturbation factors for parallel-plate chambers. [8]

The National Physical Laboratory (NPL) has introduced a calorimeter-based direct-absorbed-dose-to-water calibration service for megavoltage photon beams, and a dosimetry code of practice based on this was published by IPSM (1991). [66]

The absorbed dose to water under reference conditions in an electron beam should be determined using one of the following designated ionization chambers:

- the NE2571 cylindrical graphite-walled Farmer chamber;
- the NACP-designed parallel-plate chamber (there are two designs of this chamber, differing in their waterproofing arrangements; both are allowed);
- the Markus-designed parallel-plate chamber (PTW/Markus chamber), type 2334;
- the Roos-designed parallel-plate chamber (Roos chamber), type 34001.

The cylindrical chamber is recommended only for use in electron beams where the mean energy at the reference depth ($\bar{E}_z$) is greater than 5 MeV (in practice this typically implies that the mean energy at the surface $\bar{E}_0 \leq 10$ MeV).

A practical ionization chamber does not sample the true electron fluence which is present in the undisturbed phantom at the point corresponding to the geometrical centre of the chamber cavity. The difference between this and the fluence in the cavity depends on a number of factors, one of which is the fluence gradient across the chamber. This gives rise to the concept of the effective point of measurement P_{eff}. A practical definition of P_{eff} is that depth in the medium where the average energy is the same as in the chamber, such that stopping-power ratios as conventionally evaluated can be used.

For cylindrical chambers used in megavoltage photon and electron beams around and beyond the depth of dose maximum, a displacement of 0.6 r toward the radiation source gives a reasonable representation of the experimental data, where r is the internal radius of the cavity.

Each designated electron chamber must be calibrated in terms of $N_{D,air,ch}$, a calibration factor to convert its corrected reading to mean absorbed dose to the air in the sensitive volume. To ensure traceability to national primary standards, this calibration must be via the local standard chamber, i.e., in the UK the NPL-designed secondary-standard chamber.

For the NE2571 chamber, the $N_{D,air,2571}$ calibration is obtained by a comparison against the secondary-standard chamber with both centers at the same depth in a PMMA phantom in a ^{60}Co γ-or megavoltage x-ray beam. For parallel-plate chambers, $N_{D,air,pp}$ is obtained by comparison with an $N_{D,air}$-calibrated NE2571 chamber in a higher-energy electron beam.

The secondary-standard and the NE2571 should be placed with their centers at a depth of 5 cm in a PMMA phantom of at least 20 cm × 20 cm in area and at least 12 cm thick. They should be irradiated in a ^{60}Co beam using a 10-cm × 10-cm field at a source-to-surface distance of at least 80 cm (if a ^{60}Co beam is not available). No corrections for ambient temperature and pressure are required, provided these conditions remain stable throughout the measurements.

Ion recombination corrections are negligible in these conditions for ^{60}Co-beam measurements and may be ignored.

The $N_{D,air}$ factor for the NE2571 chamber is given by

$$N_{D,air,2571} = 0.978\ N_{K,sec}(M_{sec}/M_{2571}) \qquad (2.38)$$

where 0.978 is the combined correction factor $[(1-g) \times k_{sec}(p^{\lambda}_{sec}/p^{\lambda}_{cyl})_{PMMA}]$. $N_{K,sec}$ is the in-air air-kerma calibration factor for the secondary standard at ^{60}Co γ- or 2-MV x-rays as supplied by the national standards laboratory. The units of $N_{D,air,2571}$ are grays (absorbed dose to air) per chamber reading when $N_{K,sec}$ is in grays (air kerma) per chamber reading. The response of the parallel-plate chamber and the NE2571 should be determined in turn at the reference depth in a high-energy electron beam. The beam should have an $\bar{E}_0$ of preferably 17–22 MeV and no less than 15 MeV in order to maintain the in-scattering correction ($p^{e}_{cav,cyl}$) for the Farmer chamber within 2% of unity and thus to minimize its uncertainty.

TABLE 2.1
Ratios of the Linear Continuously Slowing Down Range r_0/ρ[a] as a Function of Electron Energy for Different Plastics to the Corresponding Values for Water[b]

$\bar{E}_0$ (MeV)	A−150	Polystyrene	PMMA
0.1	0.879	0.961	0.863
0.2	0.880	0.963	0.864
0.5	0.882	0.964	0.864
1.0	0.886	0.967	0.865
2	0.891	0.970	0.867
5	0.897	0.974	0.870
10	0.902	0.978	0.872
15	0.906	0.983	0.874
20	0.909	0.987	0.876
30	0.914	0.993	0.878
40	0.919	0.999	0.882
50	0.922	1.003	0.883

[a] Note that r_0 conventionally is given in units of g cm^{-2}, while R_t, R_{50}, and R_p generally are given in cm.

[b] The density of plastic may vary from one sample to another. It is therefore recommended that the density is measured and corrections are applied if necessary to the figures given in the table.

Source: From Reference [64]. With permission.

The irradiations should preferably be carried out in a water phantom. It is important to allow phantoms and chambers to reach thermal equilibrium before measurements are begin.

The readings for each chamber should be corrected for polarity and ion recombination. The $N_{D,air}$ for the parallel-plate chamber is given by

$$N_{D,air,pp} = M_{2571} N_{D,air,2571} \, p^e_{cav,2571}(\bar{E}_z)/M_{pp} p^e_{pp}(\bar{E}_z) \tag{2.39}$$

where M_{2571} and M_{pp} are the readings of the chambers for the same number of mitor units and corrected as mentioned above. $p^e_{cav,2571}$ is the in-scattering perturbation factor for the NE2571 in this electron beam at this depth (i.e., at the appropriate $\bar{E}_z$).

The densities for A-150, polystyrene, and PMMA were 1.127, 1.06, and 1.19 g cm^{-3}, respectively:

$$\frac{R_{pl}}{R_w} = \frac{(r_0/\rho)_{pl}}{(r_0/\rho)_w} \tag{2.40}$$

values of r_0/ρ ratios for three materials as shown in Table 2.1.

The effect of a nonstandard SSD on machine output and dose distributions must be assessed in order to assure proper patient treatment. The majority of nonstandard SSD treatments are at an extended SSD, and as a general rule one should avoid such treatments unless absolutely necessary. Detailed calculations or measurements are required for individual machines and circumstances Khan et al. [9].

The relationship between maximum dose at the nominal (calibration) SSD and the maximum dose at the extended SSD is called the output correction. Two methods of output correction are typically used, namely, the effective SSD method and the virtual SSD method. In the effective SSD method, the dose D'_{max} at an extended SSD' is related to the dose D_{max} at the nominal SSD by the following inverse-square law relationship:

$$D'_{max} = D_{max} \frac{(\text{SSD}_{eff} + d_{max})^2}{(\text{SSD}_{eff} + g + d_{max})^2} \tag{2.41}$$

Where SSD_{eff} is the effective SSD for calibration for the given collimator field size and energy, g equals the difference between SSD' and SSD, and d_{max} is the depth of maximum dose on the central axis. As stated earlier, the inverse square law relationship may not be exactly followed for the treatment conditions involving low electron energies and large air gaps. In those cases, either the $(Q_0/Q_g)^{1/2}$ vs. g data measured for various field sizes, electron energies, and air gaps may be used directly or a new calibration may be performed for the given treatment conditions.

The use of an extended treatment distance has only minimal effect on the central-axis depth dose and the off-axis ratios. Under the treatment conditions in which the dose rate changes with the effective SSD in accordance with the inverse-square law, the depth-dose distribution can be calculated according to

$$\%D(d, \text{SSD}, g) = \%D(d, \text{SSD}, 0) \times \frac{[(\text{SSD}_{eff} + d)/(\text{SSD}_{eff} + g + d)]^2}{[(\text{SSD}_{eff} + d_{max})/(\text{SSD}_{eff} + g + d_{max})]^2} \tag{2.42}$$

where the depth dose equals 100% at d_{max} for both standard and extended SSD. For typical values of SSD_{eff}, g, d, and d_{max}(SSD_{eff} = 100 cm, d_{max} = 2 cm, $g < 10$ cm, $d < 15$ cm), this correction will have an insignificant effect (< 1 mm) on the shape of the depth-dose curve (< 1 mm shift on descending portion) so that the use of the standard depth-dose curve should be an acceptable approximation at extended distances.

The mean electron energy at the surface of the phantom is $\bar{E}_0$. The relationship between $\bar{E}_0$ and R_{50} is usually taken to have the general form

$$\bar{E}_0 = C \, R_{50} \tag{2.43}$$

where C is a constant.

TABLE 2.2
The Relationship Between the Mean Energy at the Phanton Surface, $\bar{E}_0$, and the Half-Value Depths $R_{50,D}$ or $R_{50,I}$ Measured from Broad-Beam Absorbed Dose and Ionization Curves, Respectively, at $SSD = 100$ (From Reference 8 with permission)

$\bar{E}_0$ (MeV)	$R_{50,D}$ (cm)	$R_{50,I}$ (cm)
2	0.7	0.7
3	1.2	1.2
4	1.6	1.6
5	2.1	2.1
6	2.5	2.5
7	3.0	3.0
8	3.4	3.4
9	3.8	3.8
10	4.3	4.3
12	5.1	5.1
14	6.0	5.9
16	6.8	6.7
18	7.8	7.6
20	8.6	8.4
22	9.4	9.2
25	10.7	10.4
30	12.8	12.3

When the R_{50} is taken from a dose distribution which has been obtained with a constant SSD (e.g., $SSD = 100$ cm),

$$\bar{E}_0(\text{MeV}) = 0.818 + 1.935\ R_{50,I} + 0.040(R_{50,I})^2 \tag{2.43a}$$

for $R_{50,I}$ (depth of 50% of maximum ionization) determined from a depth-ionization curve and

$$\bar{E}_0(\text{MeV}) = 0.656 + 2.059\ R_{50,D} + 0.022\ (R_{50,D})^2 \tag{2.43b}$$

for the case of $R_{50,D}$ (depth of 50% of maximum dose) determined from a depth-dose curve. As a guide, values are given in Table 2.2 for $\bar{E}_0$ from 2 to 30 MeV.

The absorbed dose to water in grays in the electron beam at the position of the effective point of measurement of the chamber when the chamber is replaced with water is given by

$$D_w(z_{ref,w}) = M^e_{ch,w} N_{D,air,ch}\ s^e_{w/air}(\bar{E}_0, z_{ref,w}) p^e_{ch}(\bar{E}_z) \tag{2.44}$$

where $M^e_{ch,w}$ is the corrected chamber reading; $s^e_{w/air}(\bar{E}_0, z_{ref,w})$ is the appropriate water-to-air stopping power ratio for an electron beam of mean surface energy $\bar{E}_0$ at depth in water $z_{ref,w}$; and $s^e_{w,air}(\bar{E}_u, z_{red,w})\, p^e_{ch}(\bar{E}_z)$ is the perturbation factor applicable to the particular ionization chamber in an electron beam at a mean energy $\bar{E}_z$ at depth $z_{ref,w}$. The $p^e_{ch}(\bar{E}_z)$ values for the Markus chamber are given by

$$p^e_{Markus} = 1 - 0.039\exp(-0.2816\bar{E}_z) \tag{2.45}$$

It is generally recommended that water phantoms should be used wherever possible for the experimental procedures involved in the absolute calibration of electron beams. However, it is recognized that in certain situations, particularly for lower-energy electron beams and the use of parallel-plate chambers, it may be more convenient to use solid plastic phantoms. In this case, the depths need to be scaled to water-equivalent depths and the chamber reading needs to be multiplied by an appropriate fluence-ratio correction.

The effective water depth, $z_{w,eff}$, which can be taken as an approximation to the depth of water which is equivalent to a given depth in a plastic phantom, can be obtained from scaling:

$$z_{w,eff} = z_{non-w} C_{pl} \tag{2.46}$$

The recommended values of the scaling factors, C_{pl}, are given in Reference [8].

The expression to evaluate the absorbed dose to water in this situation is

$$D_w(z_{ref,w}) = M^e_{ch,non-w} h_m N_{D,air,ch}\ s^e_{w/air}(\bar{E}_0, z_{w,eff}) p^e_{ch}(\bar{E}_z) \tag{2.47}$$

Electron beam absorbed dose distribution in a water phantom is shown in Figure 2.12.

The polarity correction is given by

$$f_{pol} = (|M^+| + |M^-|)/2M \tag{2.48}$$

where the superscripts + or − indicate the reading (M) with collecting voltage positive and negative, respectively, and M in the denominator is the reading taken with the normal polarity used during measurements.

In the two voltage techniques two ionization chamber readings are taken in the same irradiation conditions, one at the normal collecting voltage (V_1, reading M_1) and one at a lower voltage (V_2, reading M_2). The ratio V_1/V_2 should have a value of 2 or 3. p_{ion}, the recombination correction factor to be applied at the normal collecting voltage, can be obtained from the solutions of the particular expressions for pulsed and pulsed scanned beams. To simplify this, Weinhous and Meli [10] have given quadratic fits to these solutions:

$$p_{ion} = a_0 + a_1(M_1/M_2) + a_2(M_1/M_2)^2 \tag{2.49}$$

For small corrections ($(p_{ion} - 1) < 0.05$) the theoretical expressions reduce in a first approximation to

$$p_{ion} - 1 = (M_1/M_2 - 1)/(V_1/V_2 - 1) \qquad (2.50)$$

i.e., the percentage correction is simply the percentage change in reading divided by a number equal to one less than the voltage ratio. If the voltage ratio selected, V_1/V_2, equals 2, the percentage recombination correction is equal to the percentage change in reading. Such an approach yields values of p_{ion} accurate to 0.1% for corrections up to 3% and to 0.5% for corrections up to 5%.

For parallel-plate chambers, Boag's analytical formulas may be applied. For pulsed beams p_{ion} can be written as

$$p_{ion} = u/\ln(1 + u) \qquad (2.51)$$

where

$$u = \mu m d^2/V$$

If m is the dose per pulse in centigrays, d is the plate separation in mm, and V is the collecting voltage in volts, then μ is a constant equal to 10.7 V mm^{-2} cGy^{-1}. For cylindrical chambers the effective electrode spacing can be calculated from expressions given by Boag, and for a Farmer-designed chamber, such as the NE2571, the value obtained is 3.36 mm. Thus, the percentage loss of signal due to recombination in a Farmer 2571 chamber is calculated to be approximately 2.4% in a pulsed beam having 0.1 cGy/pulse and using a collecting voltage of around 250 V.

III. PHOTONS DOSIMETRY

The term "medium-energy x-rays" refers to x-rays of half-value layers in the range 0.5–4 mm Cu or equivalently above 8 mm Al covering approximately those generated at tube voltages in the range 160–300 kV. The recommended reference depth in this energy range is 2 cm in a full scatter water phantom. The equation for the calculation of absorbed dose at this reference depth for a given field size is

$$D_{w,z=2} = MN_K k_{ch}\left[\left(\frac{\bar{\mu}_{en}}{\rho}\right)_{w/air}\right]_{z=2,\Phi} \qquad (2.52)$$

where $D_{w,z=2}$ is the dose to water in grays at the position of the chamber center at a depth $z = 2$ cm when the chamber is replaced by water. M is the instrument reading obtained with a chamber corrected to standard pressure and temperature (20°C, 1013.25 mbar, and 50% relative humidity); N_K is the chamber calibration factor in grays per scale reading to convert the instrument reading at the beam quality (HVL) concerned to air kerma free in air at the reference point of the chamber with the chamber assembly replaced by air; $[(\mu_{en}/\rho)_{w/air}]_{z=2,\Phi}$ is the mass energy absorption coefficient ratio, water to air, averaged over the photon spectrum at a water depth of 2 cm and field diameter Φ; and k_{ch} is a factor which accounts for the change in the response of the ionization chamber between calibration in air and measurement in a phantom.

The recommended procedure for the intercomparison (in water) of a field instrument with a secondary-standard dosimeter (i.e., the determination of the product $[N_K k_{ch}]_f$ for the field instrument) is given below. The intercomparison should be carried out using the same x-ray facilities and radiation qualities as will subsequently be measured by the field instrument.

Measure the first half-value layer (HVL_1) for each radiation quality and determine the secondary-standard calibration factor N_K by interpolation from those given by the standards laboratory. Intercompare the secondary-standard dosimeter and the field instrument by simultaneous irradiation in a water phantom, following the procedures specified below. A "solid water" phantom may be used, provided that a previous, independent intercomparison in this quality range has been made in both the "solid" and natural water phantoms and any necessary corrections applied. A Perspex phantom is not recommended. The phantom should extend outside the beam edges and at least 10 cm beyond the chamber center along the beam axis. The front surface of the phantom should be at the standard source-surface distance (SSD) for the applicator. The field size for the comparison should be 10 cm × 10 cm (at the front surface of the phantom) and the reference points of the two chambers should be at the same depth of 2 cm in water. An appropriate separation of the chamber centers is 3 cm, with each chamber equidistant from the beam axis. If the intercomparison is in water, waterproof sheaths should be used.

The dose in water (indicated here by w) is determined at a depth z of 2 cm. This was chosen because this depth is more relevant in the clinic than that of 5 cm and also because of the rapid reduction of the dose with depth in the kV region. The dose $D_{w,z=2}$ is given by Equation (2.52). The overall correction factor k_{ch} which takes account of various effects, including the modification of the spectrum (primary) by 2 cm of water, the attenuation and scattering by the material (water in this case) in the hole. Figure 2.13 compares the values recommended in the IPEMB CoP with both the original IAEA [64] and the revised IAEA (1993) figures; the dashed line serves to emphasize that this factor was implicitly assumed to be unity in ICRU. [11]

For the determination of the absorbed dose to any medium *med* on the surface of a phantom made of that medium, the following relation [12],

$$D_{med,z=0} = MN_K B_{med}\left[\left(\frac{\bar{\mu}_{en}}{\rho}\right)_{med,air}\right]_{air} \qquad (2.53)$$

is used, where M is the in-air chamber reading corrected for temperature and pressure, N_K is the air-kerma calibration

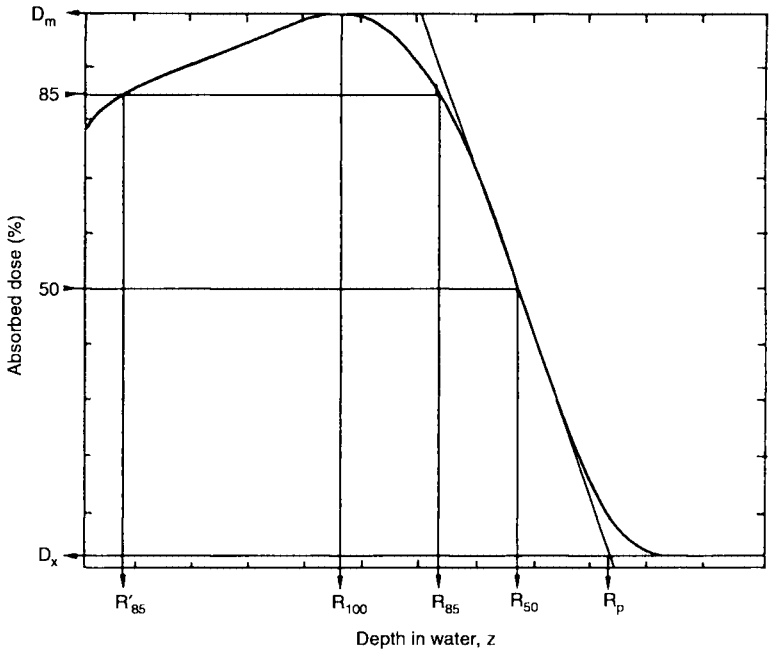

FIGURE 2.12 An electron beam absorbed dose distribution in a water phantom: D_m is the maximum absorbed dose; D_x I is the absorbed dose due to *bremsstrahlung*; R_{100} is the depth of dose maximum; R_{85} is the therapeutic range (it is here assumed that $R_t = R_{85}$; the depth at which the therapeutic interval intersects the depth dose curve near the skin entrance is designated by R'_{85}); R_{50} is the depth for 50% absorbed dose; and R_p is the practical range.

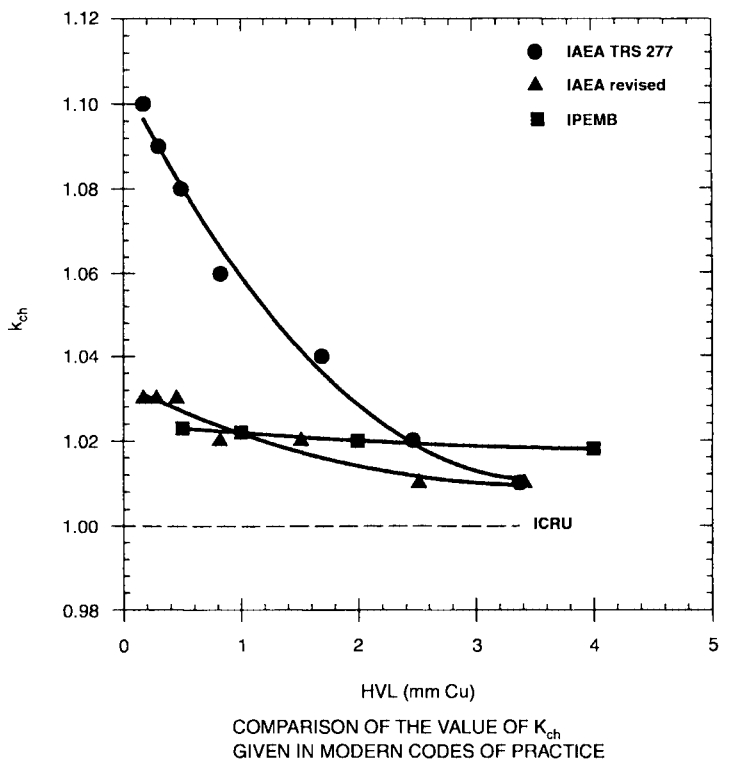

FIGURE 2.13 Comparison of the value of K_{ch} given in modern codes of practice (From Reference [11]. With permission.)

factor, B_{med} is the backscatter factor defined as the ratio of the collision kerma to the phantom material at a point on the beam axis at the surface of a full scatter phantom, to the collision kerma to the same material at the same point in the primary beam with no phantom present, and $[(\bar{\mu}_{en}/\rho)_{med,air}]_{air}$ is the ratio of the mass energy- absorption coefficients for the phantom material to air averaged over the primary photon spectrum. An advantage of the above formalism [Equation (2.53)] over the previous formalism is that by changing the definition of the backscatter factor from air-kerma ratio to water-kerma ratio, the mass energy–absorption coefficient ratio, water to air, becomes independent of phantom scatter. Thus, it is field size–independent.

Equation (2.53) determines kerma to the medium at $z = 0$ rather than absorbed dose to the medium, as the latter is highly affected by electron contamination and electron build-up. In general, charged particle equilibrium (CPE) does not exist on the surface. The dose to the medium at a depth where CPE has just been established is a more meaningful quantity for clinical radiotherapy and its value is practically the same as the surface kerma.

To determine the absorbed dose to any medium, *med*, at a reference depth (e.g., 2 cm) in that medium using an ionization chamber, the relation

$$D_{med,z=2} = MN_K P_{Q,cham} P_s \left[\left(\frac{\bar{\mu}_{en}}{\rho}\right)_{med,air}\right]_{z=2} \tag{2.54}$$

can be used where M is the in-phantom chamber reading corrected for temperature and pressure, N_K the air kerma calibration factor, $P_{Q,cham}$ the overall correction factor which accounts for the effects of the change in beam quality between chamber calibration and measurement and the perturba-tion due to the introduction of the chamber in the medium, P_s the water proofing sleeve correction factor, and $[(\bar{\mu}_{en}/\rho)_{med,air}]_{z=2}$ the mass energy–absorption coefficients for the medium to air averaged over the spectrum present in undisturbed medium at the depth of the chamber center.

The percentage depth dose (*PDD*) is defined as

$$PDD(z) = \frac{D_{med,z}}{D_{med}(max)} \times 100\% \tag{2.55}$$

where $D_{med}(max)$ is the maximum dose in the phantom, which is usually taken as the dose on the surface $D_{med,z=0}$ for kilovoltage x-ray beams. For convenience, 100% is ignored in the following derivations. Therefore,

$$PDD(z) = D_{med,z}/D_{med,z=0} \tag{2.56}$$

Substituting Equation (2.54) into Equation (2.56),

$$PDD(z) = \frac{M_z[P_{Q,cham}]_z\left[\left(\frac{\bar{\mu}_{en}}{\rho}\right)_{w,air}\right]_z}{M_{z=0}[P_{Q,cham}]_{z=0}\left[\left(\frac{\bar{\mu}_{en}}{\rho}\right)_{w,air}\right]_{z=0}} = \frac{M_z}{M_{z=0}} C_z \tag{2.57}$$

where

$$C_z = \frac{[P_{Q,cham}]_z\left[\left(\frac{\bar{\mu}_{en}}{\rho}\right)_{w,air}\right]_z}{[P_{Q,cham}]_{z=0}\left[\left(\frac{\bar{\mu}_{en}}{\rho}\right)_{w,air}\right]_{z=0}} \tag{2.58}$$

is the *PDD* correction factor for an ion chamber in water. As P_s is almost independent of phantom depth, it has been omitted in Equation (2.58). C_z is detector-dependent and may deviate from unity significantly. So far there has been no study on C_z in the literature. [12]

One can then relate the dose anywhere in the phantom to the dose on the surface or at the reference depth using the PDD data; i.e.,

$$D_{med,z} = D_{med,z=0} PDD(z) \tag{2.59}$$

based on the "in-air" method or

$$D_{med,z} = D_{med,z=ref} PDD(z)/PDD(z = ref) \tag{2.60}$$

based on the "in-phantom" method.

To study the consistency of the two methods, Ma et al. [12] calculated the ratio R of the doses at the same depth determined by Equations (2.59) and (2.60):

$$R = \frac{D_{med,z=0}}{D_{med,z=2}} PDD(z = ref) \tag{2.61}$$

If the ratio R is unity, the "in-air" and "in-phantom" procedures are consistent with each other. It is interesting to see that no matter at what depth we compare the dose values, the consistency remains the same and is determined by the accuracy of the dose at the reference points ($z = 0$ and $z = ref$) and of the *PDD* at the ref depth. If both the dose on the surface and at the ref depth are accurately known, Equation (2.61) becomes truly a test for the *PDD* data. By substituting Equations (2.53), (2.54),

and (2.57) into Equation (2.61), we have

$$R = \frac{M_{air}B_{med}\left[\left(\frac{\bar{\mu}_{en}}{\rho}\right)_{med,air}\right]_{air}}{M_{z=ref}P_{Q,cham}\left[\left(\frac{\bar{\mu}_{en}}{\rho}\right)_{med,air}\right]_{z=ref}} PDD(z = ref) \tag{2.62}$$

The parallelism between existing air kerma formalisms based on the "absorbed dose to air" chamber factor, N_D (or N_{gas}), and the simpler approach based on calibrations in terms of absorbed dose to water, N_w, was described by Andreo. [13] The importance of avoiding steps performed by the user that introduce avoidable uncertainties in the dosimetric procedure was emphasized.

A simple relation can be given as the basis of the formalism, based on the calibration of an ionization chamber at Standard Dosimetry Laboratories in terms of absorbed dose to water, D_w, at a certain radiation quality, Q_0 (usually ^{60}Co gamma-rays):

$$D_{w,Q_0} = M_{Q_0}N_{w,Q_0} \tag{2.63}$$

This expression is based directly on the definition of the calibration factor, N_w. The main advantage of Equation (2.63) is that N_w is obtained with better accuracy than if it is derived through successive steps from the air kerma formalism. It has the simplicity that the absorbed dose to water at another photon beam with quality Q will be obtained with a relation of the type

$$D_{w,Q_0} = M_Q N_{w,Q_0}k_Q \tag{2.64}$$

where M_Q is the electrometer reading in the user's photon beam (corrected for influence quantities of a different nature, such as temperature, pressure, humidity, etc.) with the ionization chamber positioned in a water phantom, and N_w is the absorbed dose to water calibration factor supplied by the Standard Dosimetry Laboratory for the reference quality Q_0. The factor k_Q, corrects the calibration factor for differences in beam quality between the laboratory and the user. Other advantages of the method are the use of only one quantity (absorbed dose to water) along the dosimetry chain and very similar experimental conditions both at calibration and during user's measurements.

Two steps are generally required to obtain D_w from measurements in a water phantom with a chamber having a calibration factor N_K. In the first step, the (free in air) air kerma, k_{air,Q_0} is related to the mean absorbed dose D_{air,Q_0} inside the air cavity of the user's ionization chamber at the calibration quality Q_0 using

$$\bar{D}_{air,Q_0} = k_{air,Q_0}(1 - g)k_{att}k_m k_{cel} \tag{2.65}$$

where k_{att} is a factor that takes into account the attenuation (absorption and scattering) of ^{60}Co-gamma-rays in the chamber material during the calibration in a ^{60}Co beam; k_m takes into account the deviations from air equivalence of the chamber wall and build-up cap material; k_{cel} accounts for similar deviations in the material of the central electrode; and g is the fraction of the energy of the photon-produced charged particles expended in radiative processes (mainly *bremsstrahlung* in air). Specifically, k_m takes into account the lack of equivalence to air of the materials in the ionization chamber and therefore should include k_{cel}. This would allow unambiguous comparisons between experimental and calculational procedures.

An "absorbed dose to air" chamber factor, N_D, is defined as

$$\bar{D}_{air,Q_0} = N_{D,Q_0}M_{Q_0} \tag{2.66}$$

where M_{Q_0} is the meter reading of the ionization chamber system (corrected for influence quantities) in the calibration beam.

The equations above yield

$$N_{D,Q_0} = N_{K,Q_0}(1 - g)k_{att}k_m k_{cel} \tag{2.67}$$

The basic assumption in the "absorbed dose to air" chamber factor formalism is that N_{D,Q_0} is also valid at the user's beam quality Q; i.e., $N_{D,Q_0} = N_{D,Q}$. The mean absorbed dose inside the air cavity, $\bar{D}_{air,Q_0}$, can be written as

$$\bar{D}_{air,Q_0} = \frac{M_Q}{V\rho_{air}}\frac{W_Q}{e} \tag{2.68}$$

where M_Q is the electric charge produced in the ionization chamber, V is the cavity volume and W/e is the mean energy expended in air per ion formed divided by the charge of the electron. The above assumption holds only if $W_{Q_0} = W_Q$ and implies that N_D is a function only of the mass of air inside the cavity ($V\rho_{air}$) and therefore is a constant of the chamber.

In the second step, the Bragg-Gray equation is used to determine the absorbed dose to water at the effective point of measurement, P_{eff}, from the mean absorbed dose to air $\bar{D}_{air,Q}$. Alternatively, a displacement factor P_{displ} can be used and D_w is determined at the position of the geometrical center of the chamber using

$$D_{w,Q} = \bar{D}_{air,Q_0}(s_{w,air})_Q p_Q = N_D M_Q(s_{w,air})_Q p_Q \tag{2.69}$$

where $(s_{w,air})_Q$ is the water to air stopping-power ratio and p_Q is a perturbation factor to correct for all the different contributions to the departure from ideal Bragg-Gray conditions, when an extended non-water-equivalent walled

detector is introduced in the medium, all of them given at the user's beam quality Q.

When an ionization chamber has independent calibration factors both in terms of air kerma N_K (or exposure N_x) and in terms of absorbed dose to water N_w at the same reference beam quality Q_0, it is possible to obtain a relationship between both calibration factors. Equating the absorbed dose to water at a quality Q reference point, obtained using the "absorbed dose to air" chamber factor formalism above, with that used in Equation (2.64) results in

$$N_{w,Q_0} = N_{k,Q_0}(1-g)k_{att}k_m k_{cel}(s_{w,air})_{Q_0}P_{Q_0} \qquad (2.70)$$

and the factor k_Q in Equation (2.64) becomes

$$k_Q = \frac{(S_{w,air})_Q}{(S_{w,air})_{Q_0}} \frac{p_Q}{p_{Q_0}} \frac{W_Q}{W_{Q_0}} \qquad (2.71)$$

which explicitly includes the quality dependence of W; the meanings of the factors $S_{w,air}P_Q$ and W have been given above. [13]

A quality index can be used to define the absorbed dose to water if its energy dependence is known.

Three parameters, HVL, mean energy at a depth of 2 cm in water, and the ratio of the doses at depths of 2 and 5 cm in water (D_2/D_5) were investigated by Rosser [14] as functions of $[(\bar{\mu}_{en}/\rho)_{w/a}]_{z=2,\phi}$. The quality index that best defines $[(\bar{\mu}_{en}/\rho)_{w/a}]_{z=2,\phi}$ is the ratio of doses at depths of 2 and 5 cm in water.

$[(\bar{\mu}_{en}/\rho)_{w/a}]_{z=2,\phi}$ varies by 5.8% between 0.47 and 4 mm Cu HVL. Therefore, the energy-dependent factor of the absorbed dose to water will be taken as being the same as that for $[(\bar{\mu}_{en}/\rho)_{w/a}]_{z=2,\phi}$.

There are two practical problems associated with this quality index. First, it is not easy to measure the absorbed dose to water at a depth in water. The ratio of doses at water depths of 2 and 5 cm (D_2/D_5) is given by:

$$\frac{D_2}{D_5} = \frac{(MN_K k_{ch}[(\bar{\mu}_{en}/\rho)_{w/a}])_2}{(MN_K k_{ch}[(\bar{\mu}_{en}/\rho)_{w/a}])_5} \qquad (2.72)$$

For general dosimetry, k_{depth} is negligible. Therefore, Equation (2.72) reduces to:

$$\frac{D_2}{D_5} = \frac{M_2}{M_5}k_{depth} \qquad (2.73)$$

thus showing that D_2/D_5 may be a practical quality index.

The absorbed-dose calibration service from National Physical Laboratory (NPL) is based on a primary-standard calorimeter that measures absorbed dose to graphite. Secondary-standard dosimeters are calibrated in absorbed dose to water in a ^{60}Co gamma-ray beam and in x-ray beams over a range of generating potentials from 4 MV to 19 MV. Two methods were used by Burns [15] to convert the calibrations of working-standard ionization chambers from absorbed dose to graphite into absorbed dose to water. One method involved the use of published interaction data for photons and secondary electrons and required a knowledge of the chamber construction. The second method involved the calculation of the ratio of absorbed dose in graphite and water phantoms irradiated consecutively in the same photon beam using the photon-fluence scaling theorem. The two methods were in agreement to 0.1%.

There are three stages to the calibration procedure of NPL:

1. Working-standard ionization chambers in a large graphite phantom are calibrated in absorbed dose to graphite, N_c, by comparison with the primary-standard graphite calorimeter.
2. The calibration factors of the working-standard chambers in absorbed dose to graphite, N_c, are converted into calibration factors in absorbed dose to water, N_w, with the chambers in water, using conversion factors derived from a program of work.
3. Secondary-standard chambers are calibrated in absorbed dose to water by comparison with the working-standard chambers in a water phantom.

A group of three NE2561 ionization chambers is kept at NPL and these chambers are used as working standards. These are recalibrated once a year in a graphite phantom by direct comparison with the calorimeter over the whole range of energies. NE2561 chambers were chosen as working standards because of their known long-term stability.

The calibration of the working standards in comparison with the calorimeter is in terms of absorbed dose to graphite, whereas the quantity required for the calibration of secondary-standard dosimeters for use in radiotherapy is absorbed dose to water. The subscript following a symbol indicates the particular medium to which the physical quantity represented by the symbol applies: c = graphite, w = water, and P = Perspex. The formula used to calculate the ratio of calibration factors N_w/N_c for a working-standard ionization chamber exposed in water and graphite to a beam of high-energy photons is given by Equation (2.74). The point of measurement is taken as the center of the chamber.

$$\frac{N_w}{N_c} = \frac{k_w}{k_c}\frac{p_w}{p_c}\frac{s_w}{s_c}\frac{(\bar{\mu}_{en}/\rho)_w}{(\bar{\mu}_{en}/\rho)_c}\frac{\beta_w}{\beta_c} \qquad (2.74)$$

where k is the photon energy-fluence rate at the center of the chamber collecting volume divided by the ionization current, p corrects for the replacement of the medium by

the chamber cavity and wall, s corrects for the replacement of the medium by the chamber stem, $\bar{\mu}_{en}/\rho$ is the mean mass energy-absorption coefficient for the photons at the point of measurement, and β is the absorbed dose at the point of measurement divided by the collision kerma at the same point.

For a graphite-walled chamber which is fitted with a Perspex waterproof sheath when the chamber is in water, k_w/k_c is given by

$$\frac{k_w}{k_c} = \left(\alpha_{wall} + \alpha_{sheath}\frac{(\mu_{en}/\rho)_p(L/\rho)_c}{(\mu_{en}/\rho)_c(L/\rho)_p} + \alpha_{wall}\frac{(\bar{\mu}_{en}/\rho)_w(L/\rho)_c}{(\mu_{en}/\rho)_c(L/\rho)_w}\right)^{-1} \tag{2.75}$$

where α is the fraction of ionization in the cavity arising from photon interactions in the component indicated by the subscript and L/ρ is the mean restricted mass collision stopping power for secondary electrons.

The absorbed dose calibration factor is defined by $N_m = D_m/Q_m$, where D_m is the absorbed dose to the medium at a point corresponding to the center of the chamber with the chamber replaced by the medium, and Q_m is the charge produced by the ionization in the cavity of the chamber. Hence, the ratio of calibration factors of the chamber in water and graphite is given by

$$\frac{N_w}{N_c} = \frac{D_w/Q_w}{D_c/Q_c} = \frac{D_w}{D_c}\frac{Q_c}{Q_w} \tag{2.76}$$

To show how the photon-fluence scaling theorem is applied, it is necessary to first convert the ratio of absorbed doses into a ratio of photon energy fluences. The relationship between absorbed dose D_m and photon energy fluence Ψ_m at a point in a medium m irradiated by a photon beam under conditions of transient electron equilibrium is

$$D_m = \Psi_m(\bar{\mu}_{en}/\rho)_m\beta_m \tag{2.77}$$

Hence, the ratio of absorbed dose at given points in the two media is

$$\frac{D_w}{D_c} = \frac{\Psi_w}{\Psi_c}\frac{(\bar{\mu}_{en}/\rho)_w}{(\bar{\mu}_{en}/\rho)_c}\frac{\beta_w}{\beta_c} \tag{2.78}$$

Thus, from Equation (2.76),

$$\frac{N_w}{N_c} = \frac{\Psi_w}{\Psi_c}\frac{Q_c}{Q_w}\frac{(\bar{\mu}_{en}/\rho)_w}{(\bar{\mu}_{en}/\rho)_c}\frac{\beta_w}{\beta_c} \tag{2.79}$$

Values of N_w/N_c for the working-standard chambers derived from the two conversion methods are in excellent agreement with each other over the range of beam energies covered by the NPL calibration service, as shown in Figure 2.14.

A dose calculation algorithm has been developed by Chui et al. [16] for photon beams with intensity modulation generated by dynamic jaw or multileaf collimations. The correction factors are used to account for the effect of the intensity distribution of a beam and are calculated, at

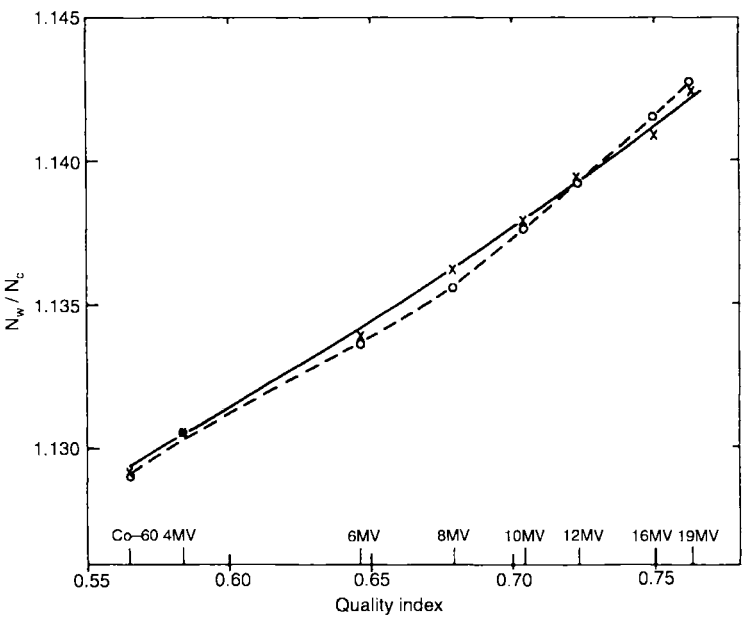

FIGURE 2.14 Comparison of N_w/N_c for NE2561 chamber derived by both methods. Crosses and continuous line are derived from dose-ratio method; circles and dashed line are derived from cavity-ionization theory method. (From Reference [15]. With permission.)

each point, as a ratio of the dose resulting from an "idealized" dynamic-collimated field to that from the corresponding "idealized" static-collimated field. The dose due to an idealized dynamic-collimated field is computed as

$$D'_{dynamic}(x, y, d) = \int_w \int_h \phi(x', y') k(x - x', y - y', d) dx' dy' \quad (2.80)$$

where $\phi(x, y)$ is the fluence distribution of the dynamic collimated and $k(x, y, d)$ is the pencil-beam kernel at depth d in the medium.

Similarly, doses due to a corresponding idealized static-collimated field are calculated as

$$D'_{static}(x, y, d) = \int_w \int_h U(x', y') k(x - x', y - y', d)\, dx' dy' \quad (2.81)$$

where $U(x, y)$ is a step function describing the uniform fluence distribution of a static-collimated field and the limits of integration are the same as that for the dynamic-collimated field in Equation (2.80).

The dose from a clinical, dynamic-collimated field, $D_{dynamic}$, is finally calculated by applying the correction factors to doses calculated for a clinical static-collimated filed D_{static}:

$$D_{dynamic}(x, y, d) = D_{static}(x, y, d)\left[\frac{D'_{dynamic}(x, y, d)}{D'_{static}(x, y, d)}\right] \quad (2.82)$$

The dose, D_{static}, due to a clinical, static-collimated field may be calculated by a number of calculation models based primarily on conventionally acquired beam data. For example, it can be calculated as

$$D_{static}(x, y, d) = MU \times OF_{med}(w \times h) \cdot TMR(w \times h; d) \times OCR(w \times h; x, y, d) \quad (2.83)$$

The term MU is the number of monitor units, or beam-on time. The term $OF_{med}(w \times h)$ represents the output factor at a depth, typically d_{max}, in the medium for a field of size $w \times h$, where the field dimensions w and h are the same as the integration limits used in the convolutions described above. The *TMR* term is the tissue maximum ratio measured along the central axis of the beam, and d is the equivalent depth which accounts for patient inhomogeneity correction. The *OCR* term accounts for off-axis corrections which includes effects such as "horns," variation of beam quality with off-axis distance, and penumbra region near the edge of the field.

The relationship between $\%dd(10)_x$ and the Spencer-Attix water to air restricted stopping power ratio $(\bar{L}/\rho)^{water}_{air}$ is [17]:

$$(\bar{L}/\rho)^{water}_{air} = 1.2676 - 0.002224(\%dd(10)) \quad (2.84)$$

Yang et al. [18] have shown that it is inappropriate just to use a simple $1/r^2$ correction to convert depth-dose curves calculated for parallel beams into those for a fixed SSD. It is well known that there are scatter corrections needed as well as the $1/r^2$ corrections. Yang et al.'s data suggest changes in the value of $\%dd(10)_x$ of up to nearly 2% at low energies but no significant change for beams with $\%dd(10)_x$, greater than 80%.

Figure 2.15 presents the revised data along with the revised fit to the data for the *bremsstrahlung* beams. The revised relationship is:

$$(\bar{L}/\rho)^{water}_{air} = 1.275 - 0.00231(\%dd(10)_x) \quad (2.85)$$

A convolution/superposition based-method was developed by Liu et al. [19] to calculate dose distributions and wedge factors in photon treatment fields generated by dynamic wedges.

A dose distribution $D(x, y, z)$ as a convolution or superposition between terma $T(x, y, z)$ and photon dose kernel $K(x, y, z)$ was calculated as follows:

$$D(x, y, z) = \iiint T(x', y', z') \times K(x - x', y - y', z - z') \times dx' dy' dz' \quad (2.86)$$

Terma is a product of photon energy fluence and the mass attenuation coefficient, which represents the total energy released per unit mass by photons at their initial interactions. Dose kernel describes the distribution of relative energy deposition per unit volume around the photon initial interaction site. Thus, a convolution or superposition between the two functions in Equation (2.86) yields a three-dimensional dose distribution in the irradiated volume.

The total terma was calculated from the contribution of both photon sources; i.e.,

$$T(x, y, z) = T_p(x, y, z) + T_e(x, y, z) \quad (2.87)$$

in which $T_p(x, y, z)$ and $T_e(x, y, z)$ are terma from the primary photon source and the extra-focal photon source, respectively. Both $T_p(x, y, z)$ and $T_e(x, y, z)$ were calculated as

$$T_{p,e}(x, y, z) = \sum_E \phi_{p,e}(E, x, y, z) \times E \times [\mu(E)/\rho] \quad (2.88)$$

in which $\phi_{p,e}(E, x, y, z)$ is the fluence distribution of the primary or the extra-focal sources; $\mu(E)/\rho$ is the mass

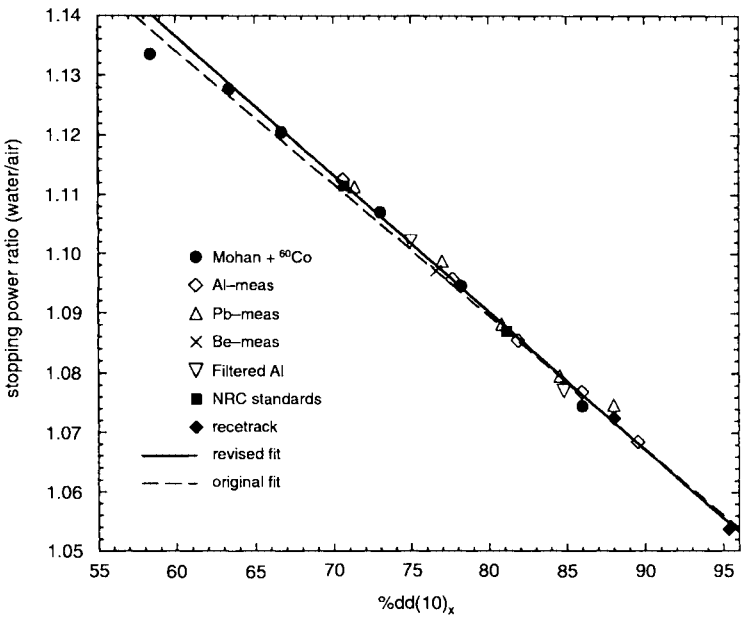

FIGURE 2.15 Calculated Spencer-Attix water to air stopping-power ratios (based on ICRU 37 stopping powers) vs. $\%dd(10)_x$. The solid straight line is the linear fit [Equation (2.85)] to the revised data for all the *bremsstrahlung* beams, whereas the dashed line is the fit to the original data. (From Reference [17]. With permission.)

attenuation coefficient of photons at energy E. The $\phi_{p,e}(E, x, y, z)$ was obtained from the results of the Monte Carlo simulation.

The total photon fluence in the dynamic field after the entire treatment being delivered can be calculated as

$$\phi(x, y) = \int s(t) \times \phi_s(x, y, t)\, dt \tag{2.89}$$

in which $s(t)$ describes the machine output per unit time at time t; $\phi_s(x, y, t)$ is the photon fluence per unit machine output in the component static field at position (x, y) and time t.

Techniques for reducing computation time in 3D photon dose calculations were addressed by Aspradakis and Redpath [20] with specific emphasis given to the convolution/superposition approach. A single polyenergetic superposition model calculating absorbed dose per incident photon fluence (Gy cm^2) was developed in terms of terma and a total energy deposition kernel (a total point spread function). A novel approach was devised for reducing calculation time. The method, named the CF method, was based on the use of a conventional, fast model for the generation of 3D dose distributions on a fine dose matrix. Superposition calculations were carried out on a coarse matrix and calculation speed was increased simply by reducing the number of calculations. A set of correction factors was derived on the coarse grid from the ratio of the dose values from superposition to those from the conventional algorithm. These were interpolated onto the fine matrix and used to modify the dose calculation from the conventional algorithm. The method was tested in a worst-case example where large dose gradients were present and in a clinically relevant irradiation geometry. It is shown that the time required for the generation of a 3D matrix with superposition can be reduced by at least a factor of 100 with no significant loss in accuracy.

The distribution of terma was calculated analytically (in voxels of 0.5 cm in all dimensions) as a product of the mass attenuation coefficient and the energy fluence at each depth. The kernels represent the energy deposited in a large water medium from a monoenergetic pencil beam of photons that experience their first interaction at the center of a large water medium. They were stored on a spherical coordinate system and their use from the dose deposition point of view was based on the reciprocity exhibited between photon interaction and dose deposition sites. Dose at $\bar{r}$ in water calculated with the superposition method is expressed by

$$D(\bar{r}) = \int_E \iiint_{volume} T_E(\bar{s}) h_{\rho_{water}}(E, \bar{r} - \bar{s})\, d^3 s dE \tag{2.90}$$

where T_E is the terma differential in energy and h is the (monoenergetic) energy deposition kernel generated in water.

The code of practice for the determination of absorbed dose for x-rays below 300 kV [21] has been approved by the IPEMB and introduces the following changes to the previous codes:

1. The determination of absorbed dose is based on the air kerma determination (exposure measurement) method.
2. An air kerma calibration factor for the ionization chamber is used.
3. The use of the F (rad/roentgen) conversion factor is abandoned and replaced by the ratio of the mass-energy absorption coefficients of water and air for converting absorbed dose to air to absorbed dose to water. Perturbation and other correction factors are incorporated in the equations.
4. New backscatter factors are recommended.
5. Three separate energy ranges are defined, with specific procedures for each range. These ranges are:

   (a) 0.5 to 4 mm Cu HVL: for this range calibration at 2 cm depth in water with a thimble ion chamber is recommended;
   (b) 1.0 to 8.0 mm Al HVL: for this range calibration in air with a cylindrical ion chamber and the use of tabulated values of the backscatter factor are recommended;
   (c) 0.035 to 1.0 mm Al HVL: for this range calibration on the surface of a phantom with a parallel-plate ionization chamber is recommended. [21]

The reading of each instrument should be corrected to a chamber temperature of 20°C and an ambient air pressure of 1013.25 mbar. Ion recombination effects are generally small for continuous radiation. If the secondary-standard dosimeter has been calibrated at the United Kingdom National Physical Laboratory (NPL), this correction is included in the calibration factor provided. A series of at least three exposures should be given to the two chambers (series a) and the ratio M_s/M_f of the readings of the two chambers should be calculated for each exposure, where M_s and M_f are the instrument readings of the secondary standard and field instrument, respectively. The chambers should then be interchanged and the readings repeated (series b). The whole procedure should be repeated at least once so that each series contains a total of at least six exposures. The standard error of the mean of either series of ratios should not exceed 0.5%. The standard error of the mean of all the ratios calculated (series a and b together) should normally be less than 1%. The true ratio of the instrument readings is given by

$$[M_s/M_f]_t = \sqrt{[M_s/M_f]_a[M_s/M_f]_b} \tag{2.91}$$

where $(M_s/M_f)_a$ is the mean of the ratios M_s/M_f for series a, $(M_s/M_f)_b$ is the corresponding mean ratio for series *b*, and $(M_s/M_f)_t$ is the true ratio of the instruments' readings. By equating the absorbed doses according to equation (2.52), the field instrument calibration factor product $(N_K k_{ch})_f$ is given by

$$(N_k k_{ch})_f = N_{K,s} k_{ch,s} (M_s/M_f)_t \tag{2.92}$$

The field instrument calibration factor $N_{k,f}$ is given by

$$N_{k,f} = N_{K,s}(M_s/M_f)_t \tag{2.93}$$

The term "very low-energy x-rays" refers to x-rays of half-value layers in the range 0.035–1.0 mm Al, covering approximately those generated at tube voltages in the range 8–50 kV. The values of k_{ch} are not known for these energies.

In the case of low- and medium-energy x-radiation, the determination of the absorbed dose is based on treating the measuring instrument as an exposure meter by making use of the following general expression [21]:

$$D_w = X(W/e)(\bar{\mu}_{en}/\rho)_{w/air} \tag{2.94}$$

where D_w is the absorbed dose to water, X is the exposure at the point at which the dose is required, W/e is the quotient of the average energy expended to produce an ion pair in air by the electronic charge, and $(\bar{\mu}_{en}/\rho)_{w/air}$ is the ratio of the mass energy absorption coefficients of water to air averaged over the photon spectrum at the point of measurement. Air kerma has replaced exposure as the preferred quantity. The air kerma k_{air} is related to the exposure X by

$$K_{air} = X(W/e)(1/(1-g)) \tag{2.95}$$

where g is the fraction of energy of secondary charged particles lost to *bremsstrahlung* in air. It is assumed that $g = 0$; therefore, $\mu_{tr} = \mu_{en}$, and $K = K_{col}$, and $D_w = K_{col,w}$. Equation (2.94), expressed in terms of air kerma, becomes

$$D_w = K_{air}(\bar{\mu}_{en}/\rho)_{w/air} \tag{2.96}$$

$$K_{air} = MN_K \tag{2.97}$$

where N_K is the air-kerma calibration factor for the chamber, free in air at the particular HVL in question. Its purpose

is to convert the reading to air kerma at the point corresponding to the center of the chamber in the absence of the chamber, under standard ambient conditions; M is the chamber reading in the user's radiation beam.

In medium-energy x-rays

$$K_{air,hole} = MN_K k_Q \tag{2.98}$$

and, with the perturbation factor P_{dis},

$$K_{air,z} = MN_k k_Q P_{dis} \tag{2.99}$$

where $K_{air,z}$ is the air kerma at the position of the chamber center (at a depth of 2 cm) in the undisturbed medium.

The air kerma free in air, $K_{air,air}$, is converted into water kerma free in air, $K_{w,air}$, by multiplying by the water-to-air mass-energy absorption coefficient ratio for the HVL in question (note that this quantity pertains to the primary beam only and is therefore independent of field size):

$$K_{w,air} = K_{air,air}[(\bar{\mu}_{en}/\rho)_{w/air}]_{air} \tag{2.100}$$

where $(\bar{\mu}_{en}/\rho)_{w/air}$ is averaged over the photon energy spectrum in air.

The dependence of $(\bar{\mu}_{en}/\rho)_{w/air}$ on HVL is shown in Figure 2.16.

The recommended secondary-standard dosimeter for medium-energy x-ray qualities is either an NE2561, NE2611, or NE2571 ionization chamber connected to an electrometer of secondary-standard quality [21].

The recommended field instrument is any thimble ionization chamber with a volume of less than 1.0 cm^3 for which $[N_K k_{ch}]$ varies smoothly and by less than 5% over the energy range of interest, connected to any suitable electrometer. No materials with an atomic number greater than that of aluminum may be used in the vicinity of the cavity, and the chamber must be vented to the atmosphere.

The preferred chambers are the NE2505/3A, NE2571, NE2581, PTW30002, or any chambers of the "Farmer" type constructed with either a carbon wall and aluminum central electrode or with both electrodes of conducting plastic that is approximately air-equivalent. Chambers with graphite-coated nylon or PMMA walls may be vulnerable to sudden changes of response at low energies and should be used only with appropriate precautions.

The recommended secondary-standard dosimeters for low-energy x-ray qualities are NE2561, NE2611, and NE2571 ionization chambers connected to an electrometer of secondary-standard quality. The dosimeter should be calibrated in terms of air kerma, at appropriate radiation qualities, at a standards laboratory. The ionization chamber and electrometer should preferably be calibrated together.

The recommended secondary-standard dosimeter for very low-energy x-rays qualities is a PTW23342 (0.02 cm^3) or PTW23344 (0.2 cm^3) soft-x-ray ionization chamber

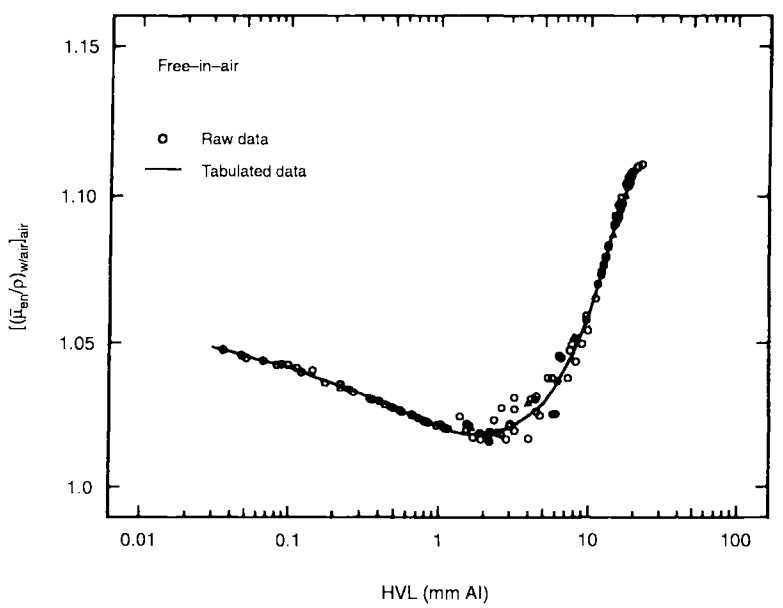

FIGURE 2.16 Mass energy absorption coefficient ratio, water to air, as a function of HVL, corresponding to the in-air (primary) spectra. (From Reference [21]. With permission.)

connected to an electrometer of secondary-standard quality.

The recommended field instruments are parallel-plate ionization chambers with volumes in the range 0.02–0.8 cm^3.

A Comparison of the IAEA 1987 and AAPM 1983 protocol

The IAEA 1987 protocol is an international protocol which has made a number of improvements over the AAPM 1983 protocol for calibration of high-energy photon and electron beams. [22] For photons, the IAEA protocol gives results which are in good agreement with the AAPM protocol; on average, the IAEA results, are 0.6% smaller than the AAPM results, while discrepancies between the two are in the range of -0.4% to -1.2%. For 10-MeV electrons also, the IAEA protocol gives results which are in excellent agreement with the AAPM protocol; on average, the IAEA results, are 0.3% smaller than the AAPM results, while discrepancies between the two are in the range of -1.0% to $+0.5\%$.

Following the formalism developed by Loevinger, the AAPM protocol introduced the concept of the cavity gas calibration factor N_{gas} for ionization chambers, as dose to the gas in the chamber divided by the electrometer reading corrected for temperature, pressure, and ionization collection efficiency; i.e.,

$$N_{gas} = D_{gas} A_{ion} M^{-1} \tag{2.101}$$

where D_{gas} is the mean absorbed dose in the cavity gas, M is the electrometer reading corrected for temperature and pressure, and A_{ion} is the ion collection efficiency in the Standards Laboratory beam.

N_{gas}/A_{ion} is a constant for a chamber and the AAPM protocol recommends that N_{gas} be determined from the ^{60}Co exposure calibration factor N_x using the following expression:

$$N_{gas} = N_x \times \frac{k(W/e)A_{ion}A_{wall}\beta_{wall}}{\alpha(\bar{L}/\rho)^{wall}_{gas}(\bar{\mu}_{en}/\rho)^{air}_{wall} + (1-\alpha)(\bar{L}/\rho)^{cap}_{gas}(\bar{\mu}_{en}/\rho)^{air}_{cap}} \tag{2.102}$$

where k is a constant equal to the charge produced in air per unit mass per unit exposure (2.58×10^{-4} C kg^{-1} R^{-1}); W/e is the quotient of the average energy expended to produce an ion pair in air by the electronic charge; A_{wall} is a factor that accounts for attenuation and multiple scattering of the primary photons in the chamber wall and the buildup cap; β_{wall} is the ratio of absorbed dose to collision part of kerma; $(\bar{L}/\rho)^{med}_{gas}$ is the ratio of the mean restricted collision mass stopping power of a medium to that of the gas in the cavity of the chamber averaged over the electron spectrum; $(\bar{L}/\rho)^{air}_{med}$ is the ratio of the average mass energy absorption coefficient for air and medium averaged over the photon spectrum; α is the fraction of ionization due to electrons from the chamber wall; and $(1-\alpha)$ is the fraction of ionization due to electrons coming from the buildup cap.

The equation for N_{gas} in the AAPM used to modify the equation for N and revised values for W/e results in cancellation of errors such that the revised values of N_{gas} are not different from the AAPM 1983 protocol values by more than 0.5%. The AAPM Radiation Therapy Committee, and the Radiological Physics Center in Houston, Texas recommended that the AAPM 1983 protocol should be used in its original form as presented in 1983.

The IAEA protocol defines an absorbed dose-to-air chamber factor N_D which has the same meaning as N_{gas} in the AAPM protocol. In the IAEA protocol, N_D is given by

$$N_D = N_k(1-g)k_{att}k_m \tag{2.103}$$

where N_k is the air-kerma calibration factor, g is the fraction of energy of the secondary charged particles that is converted to *bremsstrahlung* in air at the calibration beam, k_{att} accounts for absorption and scatter of the primary photons in the chamber wall and buildup cap, and k accounts for the lack of air equivalence of the chamber wall and buildup cap material at the ^{60}Co calibration beam and is given by

$$k_m = \alpha S_{air,wall}(\mu_{en}/\rho)_{wall,air} + (1-\alpha)S_{air,wall}(\mu_{en}/\rho)_{cap,air} \tag{2.104}$$

where $S_{air,wall}$ is the ratio of averaged stopping powers for air-to-wall material (the average is taken over the total electron energy spectrum at the point measurement in accordance with the Spencer-Attix theory); $S_{air,cap}$ has the same meaning as $S_{air,wall}$ except that the wall material is replaced by buildup cap material; $(\mu_{en}/\rho)_{wall,air}$ is the ratio of the mass energy absorption coefficient of wall to that of air; $(\mu_{en}/\rho)_{cap,air}$ is the ratio of the mass energy absorption coefficient of buildup cap to that of air; α is the fraction of ionization inside an ion chamber due to electrons arising in the chamber wall; and $1-\alpha$ is the fraction of ionization inside an ion chamber due to electrons arising in the buildup cap.

It should be noted that the IAEA protocol uses the air kerma calibration factor N_k instead of the exposure calibration factor N_x; this is in compliance with the new recommendations of the standards laboratories across

the world. The relationship between N_x and N_k is given by

$$(W/e)N_x = N_k(1 - g) \tag{2.105}$$

The AAPM protocol recommends the use of water, PMMA, or polystyrene as phantom materials for calibration of high-energy photon and electron beams. According to this protocol, the absorbed dose-to-plastic $D^{plastic}$ in the user beam quality at a reference depth d_0 is given by

$$D^{plastic}(d_0) = MN_{gas}(L/\rho)^{plastic}_{gas} P_{ion} P_{wall} P_{repl} \tag{2.106}$$

where M is the electrometer reading corrected for temperature and pressure from an ionization chamber with its center at a depth of d_0; P_{ion} is a factor that corrects for the ionization recombination loss; P_{wall} is a correction factor that accounts for differences in composition between the chamber wall and the medium; and P_{repl} is a replacement correction which accounts for the change in photon and electron fluence that occurs because of replacement of the phantom material by chamber wall and cavity.

Absorbed dose to water, D^{water}, is then calculated from

$$D^{water}(d_0) = D^{plastic}(d_0)(\bar{\mu}_{en}/\rho)^{water}_{plastic} \; ESC \text{ for photons} \tag{2.107}$$

and

$$D^{water}(d_0) = D^{plastic}(d_0)(\bar{\mu}_{en}/\rho)^{water}_{plastic} \Phi^{water}_{plastic} \text{ for electrons} \tag{2.108}$$

where $(\bar{\mu}_{en}/\rho)^{water}_{plastic}$ is the ratio of the average mass energy absorption coefficient for water to that for plastic; ESC is a correction for the fractional increase in scattered photons which occurs in polystyrene and PMMA phantoms compared to that of a water phantom; $(\bar{S}/\rho)^{water}_{plastic}$ is the ratio of the average unrestricted mass collision stopping power of water to that of plastic; and $\Phi^{water}_{plastic}$ is the ratio of electron fluence at d_{max} in water to that at d_{max} in plastic.

The IAEA protocol recommends water as the phantom material for photon beams. However, for electron beams with average energy $E_0 < 10$ MeV, both water and plastic phantoms are recommended. The absorbed dose to water in the user's beam at a reference depth of d_0 is given by

$$D_w(d_0) = M_u N_D (S_{w,air})_u P_u P_{cel} h_m \tag{2.109}$$

where N_D is the absorbed dose-to-air chamber factor and is given by

$$N_D = N_x(W/e)k_{att}k_m \tag{2.110}$$

M_u in Equation (2.109) denotes the electrometer reading corrected for temperature, pressure, humidity, and ionization recombination loss for an ionization chamber with its center at a depth of d_0 plus a fraction f of the inner radius of the chamber where $f = 0.5$ for electron beams and $f = 0.75$ for x-ray beams under investigation. $(S_{w,air})_u$ is the ratio of the average stopping power for water to air. The stopping powers are of the Spencer-Attix type. P_u is a perturbation correction to the Bragg-Gray equation and is a product of two factors which account for the lack of water equivalence of the chamber wall and the perturbation of electron fluence that occurs because of the replacement of water by chamber wall and cavity. P_{cel} is a factor that accounts for the central electrode correction; h_m is defined for electron beams only and has the same meaning as $\Phi^{water}_{plastic}$ of the AAPM protocol. It is a measured quantity and is the ratio of the signal at the ionization maximum on the central axis in water to that in a plastic phantom at the ionization maximum.

$$\frac{D_w^{IAEA}(d_0)}{D_w^{AAPM}(d_0)} = \frac{M_u}{MP_{ion}} \frac{N_D}{N_{gas}} \frac{(S_{w,air})_n}{(L/\rho)^{water}_{gas}} \frac{P_u}{P_{wall}P_{repl}} \frac{P_{cel}}{1} \tag{2.111}$$

The results of the absorbed dose intercomparison in water for all the chambers employed in this study and exposed to 4 and 25 MV photon beams are given in Table 2.3.

An equation similar to Equation (2.111) but applicable only to electron beams can be written:

$$\frac{D_w^{IAEA}(d_0)}{D_w^{APM}(d_0)} = \frac{M_u}{MP_{ion}} \frac{N_D}{N_{gas}} \frac{(S_{w,air})_u}{(\bar{L}/\rho)^{plastic}_{gas}(\bar{S}/\rho)^{water}_{plastic}} \times \frac{P_u}{P_{wall}P_{repl}} \frac{h_m}{\Phi^{water}_{plastic}} \frac{P_{cel}}{1} \tag{2.112}$$

As in the case of photons, the values of M_u, M, and P_{ion} are related to each other by the ratio of percent depth doses at $d_0 + 0.5r$ and d_0.

The AAPM protocol recommends that $\bar{E}_0$ the mean electron energy at the surface of the phantom, should be determined from the following expression:

$$\bar{E}_0 = 2.33, \quad MeVcm^{-1} \times d_{50}\,cm \tag{2.113}$$

where d_{50} in the above equation is the depth in water at which an ionization chamber reading is reduced to 50% of its maximum value. If plastic phantoms are used, then

TABLE 2.3
Absorbed Dose Intercomparison for 4- and 25-MV Photon Beams in a Water Phantom

Chamber	Photon Energy (MV)	$\frac{M_u}{MP_{ion}}$	$\frac{N_D}{N_{gas}}$	$\frac{(S_{w,air})_u}{(\bar{L}/\rho)_{air}^{water}}$	$\frac{P_u}{P_{wall}}$	$\frac{1}{P_{repl}}$	$\frac{D_{re}^{IAEA}(d_0)}{D_{ie}^{AAPM}(d_0)}$
PTW	4	0.99	1.005	0.994	1.000	1.008	0.996
Capintec	4	0.99	1.006	0.994	0.998	1.008	0.996
NEL	4	0.99	1.008	0.994	0.997	1.008	0.996
PTW	25	0.995	1.005	0.988	1.001	1.005	0.994
Capintec	25	0.99	1.006	0.988	0.999	1.006	0.988
NEL	25	0.99	1.008	0.988	1.000	1.006	0.991

Note: The values of TPR_{10}^{20} for 4- and 25-MV x-rays are 0.64 and 0.80, respectively.

Source: From Reference [22]. With permission.

d_{50} should be scaled appropriately. The AAPM provides these scale factors.

IV. STOPPING POWER

The stopping power of a material is defined as the average energy loss per unit path length that charged particles suffer as the result of Coulomb interactions with electrons and atomic nuclei when traversing the material. For protons and alpha particles, the predominant contribution to the total stopping power comes from the electronic stopping power, $-(dE/dx)_{el}$, also collision stopping power S_{col}, due to inelastic collisions with electrons. A smaller contribution comes from the nuclear stopping power, $-(dE/dx)_{nuc}$ or S_{nc}, due to elastic Coulomb collisions in which recoil energy is imparted to atoms.

The mass electronic stopping power is defined in terms of the inelastic scattering cross sections $d\sigma_{in}(W, T)/dW$ for collisions with atomic electrons:

$$\frac{1}{\rho}S_{col}(T) = NZ\int_0^{W_m} W\frac{d\sigma_{in}}{dW}\,dW \qquad (2.114)$$

where T is the initial kinetic energy and W is the energy loss of the incident particle (projectile). The upper limit of integration, W_m, is the largest possible energy loss in an inelastic collision with an atomic electron. N is the number of atoms (or molecules) per gram of material, and Z is the number of electrons per atom (or molecule).

The mass nuclear stopping power is defined in terms of the elastic scattering cross section $d\sigma_{el}(\theta, T)d\Omega$ for collisions with atoms:

$$\frac{1}{\rho}S_{nuc}(T) = 2\pi N\int_0^{W_m} W(\theta, T)\frac{d\sigma_{el}}{d\Omega}\sin\theta\,d\theta \qquad (2.115)$$

where θ is the deflection angle (in the center-of-mass system) and $W(\theta,T)$ is the recoil energy received by the target atom. The number of atoms per gram of material is

$$N = N_A/M_A = (uA)^{-1} \qquad (2.116)$$

where N_A is the Avogadro constant, M_A is the molar mass in g mol^{-1}, A is the relative atomic (or molecular) mass (sometimes denoted by A_r), and u is the atomic mass unit (1/12 of the mass of an atom of the nuclide ^{12}C).

To calculate the penetration, diffusion, and slowing down of charged particles in bulk matter, one must utilize—in principle—the complete set of differential cross sections for energy losses and angular deflections in inelastic and elastic Coulomb collisions. In the continuous-slowing-down approximation (csda), energy-loss fluctuations are neglected and charged particles are assumed to lose their energy continuously along their tracks at a rate given by the stopping power. The csda range, calculated by integrating the reciprocal of the total stopping power with respect to energy, is a very close approximation to the average path length traveled by a charged particle in the course of slowing down to rest.

In the straight-ahead approximation, the angular deflections due to multiple elastic scattering are neglected, and charged particle tracks are assumed to be rectilinear. For protons and alpha particles, this is a good approximation except near the ends of their tracks.

Stopping powers pertain to the loss of energy by the incident charged particles, whereas in radiation dosimetry, one is often more interested in the spatial pattern of energy deposition in some target region (such as an organ, cell, or cell nucleus). A large fraction of the energy lost by protons or alpha particles along their tracks is converted to kinetic energy of secondary electrons (delta-rays), and the transport of these electrons through the medium influences the spatial pattern of energy deposition. In some dosimetry calculations, the transport of energy by secondary photons (fluorescence radiation or *bremsstrahlung*) or by recoil nuclei may also have to be taken into account.